Title

MASS AND SPECTROSCOPIC MEASUREMENTS IN THE COMPLETED MASS 21 AND 37 ISOSPIN QUARTETS

Authors

Butler, Gilbert W.
Cerny, Joseph
Cosper, S.W.
et al.

Publication Date

1967-07-01

UCRL-17693

Cy. 2

University of California

Ernest O. Lawrence Radiation Laboratory

MASS AND SPECTROSCOPIC MEASUREMENTS IN THE COMPLETED MASS 21 AND 37 ISOSPIN QUARTETS

Gilbert W. Butler, Joseph Cerny, S. W. Cosper, and Robert L. McGrath

July 1967

Berkeley, California

DISCLAIMER

Submitted to Phys. Rev. Sec. 4, 1967
Index 54. 2, 5, 7, 8

UCRL-17693
Preprint

UNIVERSITY OF CALIFORNIA

Lawrence Radiation Laboratory
Berkeley, California

AEC Contract No. W-7405-eng-48

MASS AND SPECTROSCOPIC MEASUREMENTS IN THE COMPLETED MASS 21 AND 37 ISOSPIN QUARTETS

Gilbert W. Butler, Joseph Cerny, S. W. Cosper, and Robert L. McGrath

July 1967

MASS AND SPECTROSCOPIC MEASUREMENTS IN THE COMPLETED MASS 21 AND 37 ISOSPIN QUARTETS*

Gilbert W. Butler, Joseph Cerny, S. W. Cosper,† and Robert L. McGrath

Department of Chemistry and Lawrence Radiation Laboratory
University of California
Berkeley, California

July 1967

ABSTRACT

Low-lying T = 3/2 levels of the mass 21 isospin quartet (^{21}F, ^{21}Ne, ^{21}Na and ^{21}Mg) and of three members of the mass 37 quartet (^{37}Ar, ^{37}K and ^{37}Ca) have been investigated. An improved particle-identification system which employs two transmission (ΔE) and one stopping (E) detector and permits the measurement of low-yield nuclear reactions was used to determine the masses of the T_z = -3/2 nuclei ^{21}Mg and ^{37}Ca via the (^{3}He,^{6}He) reaction on ^{24}Mg and ^{40}Ca at $E_{^3He}$ = 56 MeV. Complete experimental procedures followed in these three-neutron transfer investigations are discussed. The first three T = 3/2 levels in ^{21}Ne were established by a simultaneous study of the ^{22}Ne(d,t)^{21}Ne and ^{22}Ne(d,^{3}He)^{21}F reactions at 39.6 MeV, while the ^{23}Na(p,t)^{21}Na reaction at 42 MeV was utilized to observe the lowest T = 3/2 level in ^{21}Na. Excitation energies of the lowest T = 3/2 levels in ^{37}K and ^{37}Ar were determined via the ^{39}K(p,t)^{37}K and ^{39}K(p,^{3}He)^{37}Ar reactions induced by 45-MeV protons. Data from the complete quartets were used to test the isobaric multiplet mass equation and the various predictions of masses of neutron-deficient nuclei.

I. INTRODUCTION

The measurement of masses of nuclei far from stability enables one to evaluate the various theoretical approaches toward prediction of the limits of particle stability; recent theories of interest include those of Goldansky,[1] Jänecke,[2] and Kelson and Garvey.[3] In addition, mass measurements, in conjunction with other data, permit a further study of the isobaric multiplet mass equation[4] (IMME): $M(A,T,T_z) = \underline{a}(A,T) + \underline{b}(A,T)T_z + \underline{c}(A,T)T_z^2$. Since this equation relating the masses of members of an isospin multiplet possesses three coefficients, its validity can be independently checked only if four or more members of such a multiplet with $T \geq 3/2$ are known.

We wish to report the completion of the mass 21 and mass 37 isospin quartets. Although the previous investigations of complete isospin quartets (masses 9[5,6] and 13[7]) have shown very good first order agreement with the IMME, a test among isobars possessing significantly greater Coulomb energy seemed desirable.

Although one- and two-nucleon transfer reaction investigations quite readily locate the $T = 3/2$ states in $T_z = -1/2$ and $+1/2$ nuclei, and the masses of the $T_z = +3/2$ nuclei are generally known, in order to complete the quartets it has been necessary to employ the three-neutron transfer reaction (^{3}He,^{6}He) to measure the masses of $T_z = -3/2$ nuclei. The earlier reported measurements of the $^{12}C(^3He,^6He)^9C$ and $^{16}O(^3He,^6He)^{13}O$ reactions[5,7] utilized a standard particle identifier,[8] but due to the low (^{3}He,^{6}He) cross sections ($\leq$1 μb/sr (lab) for A>16), an improved particle-identification system employing two transmission ΔE detectors and an E detector was developed.[9] This new system permitted the measurement of the masses of ^{21}Mg and ^{37}Ca via the $^{24}Mg(^3He,^6He)^{21}Mg$ and $^{40}Ca(^3He,^6He)^{37}Ca$ reactions. Excited

levels of both ^{21}Mg and ^{37}Ca were also observed in these experiments. The mass 21 ground-state analogue levels were studied through the ^{22}Ne(d,^{3}He)^{21}F, ^{22}Ne(d,t)^{21}Ne and ^{23}Na(p,t)^{21}Na reactions, while the lowest T = 3/2 levels in ^{37}K and ^{37}Ar were established by the ^{39}K(p,t)^{37}K and ^{39}K(p,^{3}He)^{37}Ar reactions.

II. EXPERIMENTAL PROCEDURE

These experiments were carried out using the external beam facilities of the Berkeley 88-inch, variable-energy cyclotron.

A. Beam Optics and General Cave Layout

Figure 1 shows the layout of the 88-inch cyclotron experimental area that was used in these studies. The beam was extracted from the cyclotron at a radius of 39.3 inches by means of a tungsten septum and an electrostatic deflector. After the beam passed through a radial collimator, a quadrupole doublet and a vertical collimator, it entered a beam analysis magnet where it was deflected toward the experimental cave. Another quadrupole lens was required to produce a further radial focus at the analyzing slit. The expected energy resolution after analysis was 0.14%. The beam was then focused to a spot typically 0.06 inch wide by 0.10 inch high in the center of a 20-inch scattering chamber by means of two additional quadrupole doublets; essentially only clean-up collimation was employed between the analysis slit and the target. Beam intensities used in these experiments varied from 50 - 800 nA, depending on the scattering angle and the reaction being studied. The accumulated beam was measured with a Faraday cup and an integrating electrometer.

The angle at which the beam passed through the center of the scattering chamber was determined by observing via remote television its impact on

luminous foils placed at the center of the chamber and 28 inches downstream. Further downstream was a foil-wheel assembly consisting of five independently rotating, 10-position metal wheels that contained varying thicknesses of aluminum. These foil wheels were used in conjunction with the Faraday cup and electrometer to measure the beam range.

The scattering chamber had two independently moveable turrets with counter axes that were either 10 deg above or below the median plane, so that scattering angles from 10 - 170 deg were observable. Counter assemblies were located just outside the scattering chamber and could be isolated from it by a vacuum valve. Rectangular tantalum collimators with approximate dimensions of 0.085 inch wide by 0.200 inch high were used and were located approximately 18.9 inches from the chamber center, giving an angular resolution (radial) of 0.26 deg and a solid angle of 5×10^{-5} sr. The counter assembly could be rotated symmetrically about its axis so that the vertical collimator height was always perpendicular to the scattering plane. When a gas target was used, an additional set of collimators (radial only) was attached to the counter assembly at a distance of 4.3 inches from the chamber center. A counter which monitored the beam energy was located in one of the viewing ports of the center stationary section of the scattering chamber. This counter was in the median plane at a scattering angle of 27.5 deg and was collimated so that it subtended approximately the same solid angle as the counter telescope systems.

A target gas cell 3.0 inches in diameter by 1.25 inches in height and with a 315 deg continuous window made of 0.1 mil Havar foil[10] (2.11 mg/cm^2) was employed when necessary. Neon gas enriched[11] to 91.3% ^{22}Ne (8.2% ^{20}Ne and 0.5% ^{21}Ne) for the study of the ^{22}Ne(d,t)^{21}Ne and ^{22}Ne(d,^{3}He)^{21}F reactions was contained in this cell at a pressure of 21 cm of Hg as measured

by a mercury manometer. A Toepler pump was used to recover the enriched neon after the experiment had been completed.

B. Procedure For High-Yield Nuclear Reactions

High-yield nuclear reactions ($d\sigma/d\Omega \gg 1$ μb/sr) were investigated utilizing two power-law type particle identifiers[8] fed by two independent ΔE-E silicon detector telescopes; a schematic diagram of one of these two systems is shown in Fig. 2. The ΔE detectors were 5.6 mil phosphorus-diffused silicon transmission counters, whereas the 120 mil E detectors, the 20 mil rejection detectors, and the various monitor detectors were all lithium-drifted silicon counters. Signals from the rejection detectors were used in anti-coincidence with those from the ΔE - E telescope to eliminate particles traversing the first two counters. Each detector was connected by a short length of low-capacity cable to the input of a fast rise-time (<10 nsec) charge-sensitive preamplifier, and via a 10 MΩ resistor to the bias supply. The preamplifiers were connected by about 150 feet of 125 Ω cable to the counting area where the signals were fed into delay-line shaped linear amplifiers. After coincidence requirements in the respective ΔE and E amplifiers were met, the amplified signals were sent to the particle identifiers. The function of these particle identifiers has been discussed in detail in Ref. 8; they work on the basis of an empirical range-energy relationship for light particles, namely $R = aE^{1.73}$, where R is the range of the particle, E is its energy, and a is a proportionality constant characteristic of the particle. A typical identifier spectrum is shown in Fig. 3. Particle-identifier pulses were fed into two four-channel routers where single-channel analyzers were set around the t, ^{3}He, and α peaks (the fourth channel was a narrow one centered about the deuteron-triton valley to make certain no tritons were lost). The energy

spectrum of a given particle was then routed into one of the four 1024-channel memory units of a 4096-channel pulse-height analyzer; data from the second counter telescope were recorded in an on-line computer which served as a second 4096-channel analyzer.

The $^{22}Ne(d,t)^{21}Ne$ and $^{22}Ne(d,^{3}He)^{21}F$ reactions were carried out with a 39.6-MeV deuteron beam. Angular distributions of reaction products from 11.6 to 41.0 deg were obtained. The $^{23}Na(p,t)^{21}Na$ and $^{23}Na(p,^{3}He)^{21}Ne$ reactions were studied at 42 MeV over an angular range of 11.4 to 40.0 deg. An evaporated, self-supporting sodium foil approximately 1 mg/cm^2 thick was transferred to the scattering chamber in an inert atmosphere, but this target oxidized to such an extent that energy levels over 11.0 MeV excitation in ^{21}Na and over 6 MeV excitation in ^{21}Ne were not observed due to very strong contaminant peaks.

The $^{39}K(p,t)^{37}K$ and $^{39}K(p,^{3}He)^{37}Ar$ reactions were studied at a proton energy of 45 MeV. The target was an evaporated, self-supporting natural potassium foil 0.8 mg/cm^2 thick that was allowed to oxidize slowly before being transferred to the scattering chamber. A small carbon impurity was also found in the target; the impurities provided convenient internal calibration points. An angular range from 14.1 to 28.0 deg was studied.

C. Procedure For Low-Yield Nuclear Reactions

Although the earlier ($^{3}He,^{6}He$) experiments[5,7] ($d\sigma/d\Omega$ (lab) ~ 1 - 4 μb/sr) employed the particle identifier described above, the presence of a relatively high background in the ^{6}He region of the identifier spectra complicated the measurements. This background arose primarily from rare events in which a few of the large number of alpha-particles stopping in the counter telescope dropped an abnormally large amount of energy in the ΔE detector (due to blocking,

Landau tail, "nuclear reactions," etc.), causing their identification signal to be significantly higher than normal. When survey experiments on the (^{3}He,^{6}He) reaction on heavier targets showed a decreasing cross section, it became necessary to develop an identification system which eliminated this background. A schematic diagram of a typical counter telescope and the electronics for this improved particle-identification system[9] is shown in Fig. 4. The counter telescope was augmented to incorporate two ΔE detectors (denoted $\Delta E2$ and $\Delta E1$) and an E detector; pulses in these detectors were amplified and fed to a fast-slow coincidence system with a fast-coincidence resolving time of 50 nsec. If the coincidence requirements were met, these three pulses were sent to the particle identifier along with timing pulses. The rejection detector performed the same function as described in the preceding section. The triple-counter identifier produced three identification pulses for each particle as schematically shown in Fig. 5; note that these identification signals were proportional to the $\Delta E2$, $\Delta E1$, and ($\Delta E2 + \Delta E1$) detector thicknesses. The first two (A, B) of these signals (which were both generated in Ident. 1 on Fig. 4) were then compared; if their ratio agreed within preset limits, a linear gate was opened allowing the third identification pulse (generated in Ident. 2 on Fig. 4) to emerge as the output of the particle identifier. Since there was only a very small chance that both ΔE signals for a particular event would deviate markedly from normal in the same direction by about the same amount, very few incorrect identifications resulted after the comparison-rejection process. Tests had shown that those particles which lost an abnormal amount of energy in a ΔE detector and were identified improperly (predominantly filling the valleys of the identifier spectrum) could be eliminated while 95 to 99 % of the total counts were retained.

The following data contrast the performance of the standard and the triple-counter identifier systems. First, Fig. 6 shows standard particle-identifier spectra from the two-neutron pick-up reaction $^{12}C(\alpha, ^{6}He)^{10}C$ at 70 MeV with $d\sigma/d\Omega_{g.s.} \sim 30 - 40$ μb/sr and from the three-neutron pick-up reaction $^{12}C(^{3}He, ^{6}He)^{9}C$ at 65 MeV with $d\sigma/d\Omega_{g.s.} \sim 1 - 4$ μb/sr. Although a ^{6}He identification peak was resolved in the former experiment, the lower cross section of the latter reaction was insufficient to cause a peak above the general background in this region of the identifier spectrum. Figure 7 is a ^{6}He energy spectrum from the $^{12}C(^{3}He, ^{6}He)^{9}C$ reaction[5] using the standard particle identifier and showing the presence of a large background. The improvement acquired with a triple-counter particle-identifier system is apparent in Fig. 8, which presents an identifier spectrum from ^{12}C + 65-MeV ^{3}He— note particularly the greatly improved peak-to-valley ratios. Finally, Fig. 9 is a ^{6}He energy spectrum from the $^{12}C(^{3}He, ^{6}He)^{9}C$ reaction obtained using the triple-counter particle-identification system and showing essentially no background.

Previous experiments had shown that chance coincidences between two particles "simultaneously" traversing the counter telescope were a significant problem in the study of low-yield nuclear reactions (see Refs. 12 and 13) in that some of these coincidences produced identification signals near those of the particles of interest. Even though a 50 nsec fast coincidence was required between the cross-over pickoff signals from the three detectors, it was found that two light particles of appropriate energies traversing the detector telescope within a time $\Delta t \leq 400$ nsec could satisfy the fast coincidence requirements because the cross-over points of all three (pile-up) energy signals were shifted in the same direction by approximately the same amount. Note Fig. 10(c), which shows a pulser-simulated triple-counter particle-identifier

spectrum for all the particle-stable nuclides from ^{3}He to ^{7}Li, while Fig. 10(b) shows the pulser-simulated particle-identifier positions of various ^{3}He + light particle (p, d, t, ^{3}He, or ^{4}He) chance coincidences, and Fig. 10(a) shows the same for various ^{4}He + light particle chance coincidences. The different particles shown in Fig. 10 were restricted to the same narrow limits of energy that were allowed experimentally in the (^{3}He, ^{6}He) investigations using the particular three-counter telescope shown in Fig. 4. As under our normal experimental conditions, a minimum energy loss of 5 MeV in the E detector was required. The silicon range-energy relations that were necessary for these calculations and for the analysis of the experimental data were coded at this laboratory[14] and agreed very well with available experimental data and prior computations.[15] It is apparent from Fig. 10 that a ^{3}He-d chance coincidence can very nearly simulate a ^{6}He-particle and an α-d chance coincidence can simulate a ^{8}He-particle.

Table I is a list of the calculated energy losses of various particles in the three-counter telescope indicated, assuming no detector dead layers. Energy losses for a ^{6}He-particle and a typical ^{3}He-d chance coincidence are listed in the upper portion of the table; although the ^{3}He-d coincidence event would be identified just above the ^{6}He region of the particle-identifier spectrum (see Fig. 10), an analysis of the ΔE2 and ΔE1 energy losses would distinguish this chance coincidence event from a ^{6}He-particle. (See Sec. D for a discussion of this procedure.) Unfortunately, not all ^{3}He-d chance coincidences can be positively distinguished from ^{6}He events, and these non-removable events appear as a background in the ^{6}He energy spectra. Also listed in the lower portion of Table I are the energy losses for a ^{8}He-particle and two sets of α-d chance coincidences—all three events having the same

total energy. The first α-d chance coincidence has ΔE2 and ΔE1 energy losses such that it could not be distinguished from the ^{8}He-particle (see Fig. 10 and Refs. 12 and 13), whereas the second α-d chance coincidence, for which only the summed energy losses are given, could be distinguished from the ^{8}He-particle by an analysis of the ΔE2 and ΔE1 energy losses.

Two approaches were followed in order to reduce these chance coincidences. First, the pile-up rejector shown schematically in Fig. 4 was designed to decrease the background due to chance coincidences. Using it, events which consisted of two particles traversing the counter telescope spaced in time by $\geq$ 47 nsec were rejected—thus restricting all chance coincidence events to those occurring in a single cyclotron beam burst. The details of this pile-up rejector are described in Ref. 9. Second, the ΔE2, ΔE1, (ΔE2 + ΔE1 + E = E_{total}), and particle identifier pulses for each event in any desired region of the identifier spectrum were recorded in an on-line PDP-5 computer via an eight-channel pulse multiplexer and a 4096 channel ADC and were later individually analyzed (see following section) using the known detector thicknesses and range-energy relations in silicon. This procedure both rejected some coincidence events and enabled us to attach a higher degree of reliability to the "good" events. Accurate analysis of these rare events of interest required two further procedures. First, a monitor detector independently measured the beam energy variation with time by recording the ^{3}He elastic scattering peak; Fig. 11(a) is a time plot of the ^{3}He beam energy as followed by the monitor detector. Second, the computer stored a pulser-simulated ^{6}He event every 12 minutes to check the entire system and provide an accurate measure of electronic drifts during the long data-collection times necessary

in the (^{3}He, ^{6}He) experiments; Fig. 11(b) shows the electronic stability of the E_{total} pulse from one triple-counter particle-identification system during a 45-hour cyclotron run.

Detector thicknesses in the triple-counter telescopes were selected to provide optimum operation only for the ^{6}He-particles and a few ^{6}Li groups from the (^{3}He, ^{6}Li) reaction, which served as a calibration reaction. Diffused-junction silicon transmission detectors were used (including the rejection detectors) to obtain minimum detector window thicknesses. Each detector was calibrated by comparing a precision pulser with the energy losses of α-particles from a ^{212}Po - ^{212}Bi natural α-source.

A 1.1 mg/cm^{2} separated-isotope ^{24}Mg foil was the target for the ^{24}Mg(^{3}He, ^{6}He)^{21}Mg reaction, which was observed in two independent systems at identical scattering angles of 14.1 deg; a 12-hour run at a beam intensity of 400 nA was required. An evaporated natural calcium foil 0.75 mg/cm^{2} thick served as the ^{40}Ca target. It was transferred to the scattering chamber in an inert atmosphere but was found to contain small amounts of ^{12}C and ^{16}O impurities. The ^{40}Ca(^{3}He, ^{6}He)^{37}Ca reaction was studied simultaneously by two independent triple-counter telescopes at identical scattering angles of 11.2 deg during a 45-hour period at a beam intensity of 400 nA (some data were also taken at scattering angles of 14.1 and 18.0 deg).

D. Data Analysis Procedures For (^{3}He, ^{6}He) Reactions

As an example of our analysis procedures for these low-yield reactions, we will utilize the data from the ^{40}Ca(^{3}He, ^{6}He)^{37}Ca experiment since it had a considerably lower cross section than the ^{24}Mg(^{3}He, ^{6}He)^{21}Mg reaction. Figure 12 presents a triple-counter particle-identifier spectrum from ^{40}Ca + 56-MeV ^{3}He-particles; the positions of ^{3}He-p, ^{3}He-d, and ^{3}He-^{3}He chance coincidences are indicated on the spectrum. The ^{3}He and ^{4}He peak heights in this spectrum are not representative since over 98% of these particles were rejected either by the rejection detector or by single channel analyzers which were set to pass only the ^{6}He and ^{6}Li ions of interest (thus recording only ^{3}He-particles between 20.0 and 24.7 MeV and α-particles between 22.3 and 27.8 MeV). Each event in the ^{6}He region of the identifier spectrum (and including the ^{3}He-p and ^{3}He-d chance coincidence regions) was routed to the on-line computer where its ΔE2, ΔE1, E_{total} and particle-identifier signals were stored on magnetic tape.

In order to discriminate between good and bad events, a plot of the ΔE2 and ΔE1 energy losses versus E_{total} for each event in the ^{6}He region of the identifier spectrum was made; such a plot for all "^{6}He" events observed in the System Two counter telescope during the ^{40}Ca(^{3}He, ^{6}He)^{37}Ca experiment is shown in Fig. 13. Events in which the ΔE2 and/or the ΔE1 energy loss deviated more than $\pm$5% from the smooth curves, which were calculated from the average detector thicknesses, were rejected (these are the circled events and they amount to about 20% of all the events) and were attributed primarily to chance coincidences. Some residual background due to non-rejectable coincidences plus other rare events remains. The peak near E_{total} channel 2160 corresponds to the ^{40}Ca(^{3}He, ^{6}He)^{37}Ca ground-state transition and the peak near channel 2040 corresponds to a transition to an excited state of ^{37}Ca;

some of the data in this figure were obtained at a scattering angle of 14.1 deg and some at a scattering angle of 11.4 deg so that these two peaks are really sharper than they appear to be. All of the valid ^{6}He events were then individually corrected for beam energy and electronic drifts (see Fig. 11) as well as for target and detector dead layer losses; the energy of each event was determined from the ^{6}He energy scale discussed below. Data from the ^{40}Ca(^{3}He, ^{6}Li)^{37}K calibration reaction was collected at intervals throughout the run to observe whether any energy shifts occurred arising from radiation damage to the counters.

The problem of establishing an absolute beam energy was treated as follows: calibration curves for ^{6}He and ^{6}Li ions were obtained by observing highly negative Q-value (α, ^{6}He) and (α, ^{6}Li) reactions on suitable targets (here ^{12}C) at angles chosen so that the ground-state groups stopped in the E detector. Since each detector was previously calibrated via a precision pulser against an α-source, an absolute α-particle beam energy of 71.0 MeV could be established from these calibrations and the known Q-value and kinematic relations, after dead layer and target losses were taken into account. (Since stopping ^{6}He-particles possessed ~30 MeV and ^{6}Li-particles ~45 MeV and since these energies were distributed among the three counters, the calibrations were such that minor extrapolations were required for the former and reasonable ones for the latter.) This α-particle beam energy agreed within 0.5% with that obtained from range-energy measurements in aluminum. The incident beam was then changed to ^{3}He-particles at the appropriate energy; this energy was again measured via aluminum range-energy measurements. More importantly, its energy was also determined from the ^{6}Li-particles from a known Q-value calibration reaction (here ^{40}Ca(^{3}He, ^{6}Li)^{37}K, see Fig. 14(b)) to be 55.9$_2$ MeV;

this was again obtained from the earlier α-source calibration and agreed with the range-energy measurements to 0.6%. This is equivalent to forcing the ^{6}Li ions from the (^{3}He, ^{6}Li) reaction to be on the same energy scale as those from the earlier (α, ^{6}Li) reaction, so that the ^{6}He ions from the (^{3}He, ^{6}He) reaction should be on the (α, ^{6}He) line established earlier. Using this procedure, an error of 1 MeV in the ^{4}He beam energy would make a difference of about 40 keV in the ^{37}Ca mass.

III. RESULTS

The results of the ^{21}Mg and ^{37}Ca mass measurements will be presented first, followed by the rest of the spectroscopic studies in the mass 21 and mass 37 isospin quartets.

A. ^{21}Mg and ^{37}Ca Mass Measurements

The mass of ^{21}Mg, which is the T_z = -3/2 member of the mass 21 isospin quartet, was determined by the ^{24}Mg(^{3}He, ^{6}He)^{21}Mg reaction at 56 MeV, and Fig. 15 shows a particle-identifier spectrum obtained during this experiment. Figure 14(a) is an energy spectrum from the ^{24}Mg(^{3}He, ^{6}Li)^{21}Na reaction, which was recorded simultaneously and used as a calibration reaction. Two independent ^{6}He energy spectra from the ^{24}Mg(^{3}He, ^{6}He)^{21}Mg reaction are shown in Fig. 16; each event in both spectra was corrected for beam energy variations, electronic drifts, and for energy losses in the target and detector dead layers. Each block represents a single event and the block width was chosen as 100 keV. There appear to be five peaks common to the two spectra which correspond to the ground state and four excited states of ^{21}Mg. The average differential

cross section for the ^{21}Mg ground-state transition at 14.1 deg (lab) was 0.84 μb/sr and the average Q-value was determined to be -27.22±0.12 MeV, which corresponds to a ^{21}Mg mass excess of 10.62±0.12 MeV (^{12}C = 0); therefore ^{21}Mg is stable to proton emission by 3.65±0.12 MeV. Average excitations of the observed ^{21}Mg excited levels were 0.22±0.03, 1.27±0.06, 1.62±0.04, and 1.89±0.04 MeV; these are consistent with the known[16] level structure of the T_z = +3/2 nucleus ^{21}F.

The mass of ^{37}Ca (T_z = -3/2) was determined via the ^{40}Ca(^{3}He,^{6}He)^{37}Ca reaction at 56 MeV. Corrected ^{6}He energy spectra from two independent observations of this reaction are shown in Fig. 17; each block represents a single event and the block width is 100 keV. Although several angles were observed in each system, all the data have been kinematically corrected to 11.2 deg. Each ^{6}He spectrum contains two sharp states which correspond to the ground and first excited states of ^{37}Ca. The average cross section for the ^{37}Ca ground-state transition at 11.2 deg (lab) was 0.175 μb/sr and the Q-value was determined to be -24.27±0.05 MeV, which corresponds to a ^{37}Ca mass excess of -13.24±0.05 MeV (^{12}C = 0). Hence ^{37}Ca is stable to proton emission by 3.2±0.2 MeV (the mass excess of ^{36}K calculated in Ref. 17 is probably good to ±0.2 MeV). The first excited state of ^{37}Ca appears at an excitation energy of 1.62±0.03 MeV, which is consistent with the known first excited state of the T_z = +3/2 nucleus ^{37}Cl at 1.72 MeV.[18]

Table II presents the forward angle center-of-mass differential cross sections for the four (^{3}He,^{6}He) reactions that have been utilized at this laboratory[5,7] for mass determinations of T_z = -3/2 nuclides. As can be noted from this table, there appears to be a marked decrease in cross section with increasing mass number A. Unfortunately, the general behavior of these

(^{3}He, ^{6}He) cross sections with angle and with bombarding energy has not been determined, so that this apparent pattern could easily be a property of our experimental conditions.

B. T = 3/2 States in ^{21}Ne and ^{21}Na

The ^{22}Ne(d,t)^{21}Ne and ^{22}Ne(d,^{3}He)^{21}F reactions were studied simultaneously to characterize the T = 3/2 states in ^{21}Ne. Triton and ^{3}He energy spectra from these reactions are shown in Fig. 18; energy resolutions (FWHM) were 160 keV for tritons and 182 keV for ^{3}He. The ground-state analogue level in ^{21}Ne was expected to lie near 8.9 MeV excitation since its analogue level in the mirror nucleus ^{21}Na appears at 8.90±0.04 MeV excitation.[19] Three sharp states at 8.92±0.025, 9.21±0.04, and 10.04±0.03 MeV were observed in the ^{22}Ne(d,t)^{21}Ne spectra; they are indicated as T = 3/2 levels in Fig. 18 and are the presumed analogues of the ^{21}F ground-, 0.28- and 1.10-MeV levels, respectively.

Angular distributions of the ^{22}Ne(d,t)^{21}Ne transitions to the ground state ($3/2^{+}$), 0.35-MeV ($5/2^{+}$), and 8.92-MeV levels, together with the distribution of the ^{22}Ne(d,^{3}He)^{21}F ground-state ($5/2^{+}$) ^{20} transition, are shown in Fig. 19; all these transitions are expected to involve L = 2 angular momentum transfers. The abscissa in Figs. 19 - 21 is the dimensionless quantity QR, where Q is the center-of-mass linear momentum transfer and R is the radius of interaction calculated from the formula $R(\text{fm}) = 1.5(A_{\text{target}})^{1/3} + 1.2$ for incident deuterons. The error bars on the data are based on counting statistics only and the absolute cross sections are expected to be accurate to ±10%. It is of particular interest to compare the ^{22}Ne(d,^{3}He)^{21}F ground-state transition with the ^{22}Ne(d,t)^{21}Ne* 8.92-MeV transition since these two

states are expected to be analogues. Assuming the charge independence of nuclear forces, transitions populating these analogue states proceed from identical initial to identical final states and hence should possess identical cross sections after phase space and isospin coupling corrections are made. These corrections involve (compare Bayman[21]);

$$\frac{\sigma(d,t)}{\sigma(d,{}^3He)} = \frac{1}{2T_a + 1} \times \frac{k(t)}{k({}^3He)} ;$$

where T_a is the isobaric spin of the target nucleus and $k(t)$, $k({}^3He)$ are the center-of-mass momenta of the particles. Noting Fig. 19 one sees that the angular distributions of the $^{22}Ne(d,t)^{21}Ne^*$ 8.92-MeV state and the $^{22}Ne(d,{}^3He)^{21}F$ ground state have similar L = 2 shapes and that their adjusted cross sections agree quite well; therefore the 8.92-MeV level of ^{21}Ne has been assigned T = 3/2 and $J^\pi = 5/2^+$ to agree with its analogue.

Angular distributions of the $^{22}Ne(d,{}^3He)^{21}F^*$ 0.28-MeV $(1/2^+)$ ^{22} transition and the $^{22}Ne(d,t)^{21}Ne^*$ 9.21-MeV transition are presented in Fig. 20. The $(d,{}^3He)$ cross sections have again been divided by 2.80 to correct for isospin coupling and phase space factors. Upon comparison of the magnitudes (and L = 0 shapes) of these two angular distributions, the 9.21-MeV level of ^{21}Ne can be assigned as a $1/2^+$, T = 3/2 state. Angular distributions of the $^{16}O(d,{}^3He)^{15}N$ ground-$(1/2^-)$ and 6.33-MeV $(3/2^-)$ states,[23] together with the distributions of the $^{22}Ne(d,{}^3He)^{21}F^*$ 1.10-MeV level and the $^{22}Ne(d,t)^{21}Ne^*$ 10.04-MeV level, are shown in Fig. 21. The spin and parity of the 1.10-MeV level of ^{21}F are not known, but when the angular distribution of this level is compared to the known L = 1 transitions to ^{15}N, it appears to possess an L = 1 shape so that it may be tentatively assigned as $J^\pi = (1/2, 3/2)^-$. The

angular distributions of the ^{21}Ne* 10.04-MeV and ^{21}F* 1.10-MeV levels (the latter cross section has been divided by the appropriate phase space and isospin coupling factor in Fig. 21) are similar in shape and have the proper relative magnitudes, so that the ^{21}Ne* 10.04-MeV state is the third T = 3/2 level in ^{21}Ne and it is also tentatively assigned spin and parity $(1/2, 3/2)^-$.

The ^{23}Na(p,t)^{21}Na and the ^{23}Na(p,^{3}He)^{21}Ne reactions were studied in order to locate T = 3/2 levels in ^{21}Na through comparison of (p,t) transitions with (p,^{3}He) transitions to the now established T = 3/2 levels in ^{21}Ne. An energy spectrum from the ^{23}Na(p,t)^{21}Na reaction is shown in Fig. 22 with typical triton energy resolution (FWHM) of 150 keV. Peak 19 in the spectrum possessed an average excitation energy of 8.92±0.03 MeV and was presumed to be the lowest T = 3/2 level since this excitation agreed with the value of 8.90±0.04 MeV reported earlier.[19] Due to the large amount of oxygen in the target, the (p,^{3}He) transitions to the ^{21}Ne analogues of the 8.92-MeV and higher levels of ^{21}Na were not observed. Several previously unreported energy levels of ^{21}Na were observed in this experiment and the results are presented in Table III along with a summary[24-26] of previously published data on states of this nucleus. No new spin and parity assignments have been made by us, and, in fact, some of the excited levels may be unresolved doublets. In general, the results of this experiment are in good agreement with the published data on the energy levels of ^{21}Na.

These new data on the mass 21 isospin quartet are summarized in Fig. 23, which shows energy level diagrams for the members of the quartet. For clarity, ground-state energies of mirror nuclei have been equated and many of the energy levels of ^{21}Ne and ^{21}Na below 10 MeV excitation have been

deleted. The four members of the completed ground-state T = 3/2 quartet are shown and T = 3/2 analogue levels are connected by dashed lines.

C. T = 3/2 States in ^{37}K and ^{37}Ar

The ^{39}K(p,t)^{37}K and ^{39}K(p,^{3}He)^{37}Ar reactions at 45 MeV were used to locate the lowest T = 3/2 levels in ^{37}K(T_z = -1/2) and ^{37}Ar(T_z = +1/2). Triton and ^{3}He energy spectra from these reactions at a laboratory angle of 26 deg are shown in Fig. 24; the energy resolutions (FWHM) were about 180 keV for tritons and 280 keV for ^{3}He-particles. Sharp states were observed in these spectra in the expected regions for the T = 3/2 levels, as predicted from Coulomb calculations and the ^{37}Cl mass, at excitations of 5.010±0.030 and 5.035±0.025 MeV in ^{37}Ar and ^{37}K, respectively. This excitation for the lowest T = 3/2 level of ^{37}K agrees with that of 5.030±0.018 MeV obtained previously.[27] Angular distributions to these two states and to the ^{37}K ground-($3/2^+$) and 1.37-MeV ($1/2^+$) states are shown in Fig. 25. Since a spin transfer of S = 0 is required to first order for (p,t) reactions, the ^{37}K* 1.37-MeV transition is expected to be a pure L = 2 transfer. Although the ^{37}K ground-state transition is allowed by angular momentum and parity selection rules to proceed via either L = 0 or L = 2 angular momentum transfers, previous (p,t) experiments[28] have shown that such transitions appear to proceed by relatively pure L = 0 transfers. Assuming the charge independence of nuclear forces, (p,t) and (p,^{3}He) transitions to T = 3/2 analogue states proceed from identical initial to identical final states primarily through only S = 0, T = 1 pick-up of two nucleons. The lowest T = 3/2 states in ^{37}K and ^{37}Ar, which are the analogues of the known ^{37}Cl ground state ($3/2^+$), should therefore have identical cross sections after isospin coupling and

phase space corrections have been made; L = 0 behavior is again expected.[28] Indeed, Fig. 25 shows that the angular distributions to these supposed analogue states possess L = 0 and are essentially identical, thereby confirming that they are T = 3/2 analogue levels with expected spins and parities of $3/2^+$.

Figure 26 summarizes the mass 37 isospin quartet data. Ground-state energies of mirror nuclei have been equated for the sake of clarity and only a few of the levels of ^{37}Ar and ^{37}K below 5 MeV excitation are shown; the level structure of ^{37}K is from Goosman and Kavanagh.[29]

IV. DISCUSSION

If the wave functions of the members of an isospin multiplet can be regarded as identical and if any charge-dependent forces are of a two-body character that can be treated as perturbations, then the masses of the members are given by the isobaric multiplet mass equation (IMME)[4];

$$M(A,T,T_z) = \underline{a}(A,T) + \underline{b}(A,T)T_z + \underline{c}(A,T)T_z^2.$$

The completion of the mass 21 and mass 37 isospin quartets permits two further independent tests of the parabolic character of the IMME since the coefficients can be determined from three of the members of a quartet and then used to predict a mass for the fourth member; we have chosen to use these data to predict the mass of the $T_z = -3/2$ nucleus in each quartet. A list of the $T_z = -3/2$ nuclei whose mass excesses have been measured, together with the coefficients and the predictions of the IMME for the four

isospin quartets which have been completed to date, is presented in Table IV. In all four of the completed isospin quartets there is very good first order agreement between the predicted and experimental mass excesses within the generally relatively large experimental errors, which indicates that the IMME is accurate over a fairly large variation in atomic number Z. An apparent discrepancy in the much more accurate mass 9 quartet data[6] was interpreted as indicating a possible (and ultimately to be expected[7]) need for the inclusion of a higher order term $\underline{d}(A,T)T_z^3$ in the IMME, but unfortunately no explicit theoretical estimate of the magnitude of such a coefficient is available. These $\underline{d}(A,T)$ coefficients of an IMME containing a $\underline{d}(A,T)T_z^3$ term were calculated from the four experimental masses in each quartet and the results are listed in Table IV; clearly such a coefficient is no greater than $\overline{Z}\alpha\underline{c}$, where $\overline{Z}$ is the average atomic number of an isospin quartet and α is the fine structure constant. Theoretical predictions of the magnitude of the expected second order corrections would be quite valuable.

Various systematic mass predictions for ^{9}C, ^{13}O, ^{21}Mg, and ^{37}Ca, together with the experimentally measured masses, are shown in Table V. Only the Kelson-Garvey predictions (Ref. 3) cover all four nuclei and their predictions appear to be in excellent agreement with the experimental masses except for ^{13}O. In general, though, all three sets of predictions are in reasonable agreement with the data and a more stringent test of such predictions would appear to require investigations of nuclei nearer proton-instability, such as ^{12}O and ^{36}Ca, which could be reached through the $(\alpha, ^{8}He)$ reaction.

ACKNOWLEDGEMENTS

The authors are indebted to F. S. Goulding and D. A. Landis for designing the pile-up rejector and other electronic equipment used in these experiments, to C. C. Maples, Jr., for developing several data analysis programs, to R. P. Lothrop and M. D. Roach for providing the transmission detectors, and to the several graduate students who aided during the long hours of data collection.

FOOTNOTES AND REFERENCES

*This work was done under the auspices of the U.S. Atomic Energy Commission.

†Present address: Physics Department, University of Southwestern Louisiana, Lafayette, Louisiana.

1. V. I. Goldansky, Nucl. Phys. 19, 482 (1960).

2. J. Jänecke, Nucl. Phys. 61, 326 (1965).

3. I. Kelson and G. T. Garvey, Phys. Letters 23, 689 (1966).

4. E. P. Wigner and E. Feenberg, Rept. Progr. Phys. 8, 274 (1941); E. P. Wigner, Proc. Robert A. Welch Foundation Conf. on Chemical Research, 1957, Vol. I, ed. by W. O. Milligan (The Robert A. Welch Foundation, Houston, 1958), p. 67; S. Weinberg and S. B. Treiman, Phys. Rev. 116, 465 (1959); D. H. Wilkinson, Phys. Letters 12, 348 (1964).

5. J. Cerny, R. H. Pehl, F. S. Goulding, and D. A. Landis, Phys. Rev. Letters 13, 726 (1964).

6. C. A. Barnes, E. G. Adelberger, D. C. Hensley, and A. B. McDonald, Proc. Int. Conf. on Nuclear Physics, Gatlinburg, Tennessee, September 1966 (to be published).

7. J. Cerny, R. H. Pehl, G. Butler, D. G. Fleming, C. Maples, and C. Détraz, Phys. Letters 20, 35 (1966).

8. F. S. Goulding, D. A. Landis, J. Cerny, and R. H. Pehl, Nucl. Instr. and Methods 31, 1 (1964).

9. F. S. Goulding, D. A. Landis, J. Cerny, and R. H. Pehl, IEEE Trans. Nucl. Sci. NS-13, No. 3, 514 (1966).

10. Hamilton Watch Company, Metals Division, Lancaster, Pennsylvania.

11. Monsanto Research Corporation, Mound Laboratory, Miamisburg, Ohio.

12. S. W. Cosper, J. Cerny, and R. C. Gatti, Phys. Rev. 154, 1193 (1967).

13. J. Cerny, S. W. Cosper, G. W. Butler, R. H. Pehl, F. S. Goulding, D. A. Landis, and C. Détraz, Phys. Rev. Letters 16, 469 (1966).

14. C. C. Maples, Jr. and J. Cerny, Lawrence Radiation Laboratory Report UCRL-17214, 1967 (unpublished).

15. C. Williamson and J. P. Boujot, Tables of Range and Rate of Energy Loss of Charged Particles of Energy 0.5 to 150 MeV, Centre D'Etudes Nucleaires de Saclay (1962); and L. C. Northcliffe, Studies in Penetration of Charged Particles in Matter, National Academy of Sciences - National Research Council, Washington, D. C. (1964), pp. 173-186.

16. Nuclear Data Sheets, Energy Levels of Light Nuclei, National Academy of Sciences - National Research Council, Washington, D. C. (1962).

17. R. E. Berg, J. L. Snelgrove, and E. Kashy, Phys. Rev. 153, 1165 (1967).

18. P. M. Endt and C. Van der Leun, Nucl. Phys. 34, 1 (1962).

19. J. C. Hardy and R. E. Bell, Can. J. Phys. 43, 1671 (1965) and references therein.

20. M. E. Bunker, M. G. Silbert, J. W. Starner, R. K. Sheline, and N. Jarmie, Bull. Am. Phys. Soc. II, 8, 317 (1963); P. Kienle and K. Wien, Nucl. Phys. 41, 608 (1963).

21. B. F. Bayman, Proc. Conf. on Isobaric Spin in Nuclear Physics, 1966, ed. by J. D. Fox and D. Robson (Academic Press Inc., New York, 1966), p. 503.

22. P. Horvat, Nucl. Phys. 52, 410 (1964); R. A. Mendelson, Jr. and R. T. Carpenter, Phys. Rev. 152, 1002 (1966); R. E. McDonald and J. A. Becker, Phys. Rev. 154, 1101 (1967).

23. The $^{16}O(d,^{3}He)^{15}N$ angular distributions at 39.6 MeV are from unpublished data of J. Cerny, et al.

24. C. Van der Leun and W. L. Mouton, Physica 30, 333 (1964).

25. J. G. Pronko, C. Rolfs, and H. J. Maier, Nucl. Phys. A94, 561 (1967) and references therein.

26. P. Bém, J. Habanec, O. Karban, and J. Němec, Nucl. Phys. A96, 529 (1967).

27. A. M. Poskanzer, R. McPherson, R. A. Esterlund, and P. L. Reeder, Phys. Rev. 152, 995 (1966) and references therein.

28. G. Bassani, Norton M. Hintz, and C. D. Kavaloski, Phys. Rev. 136, B1006 (1964); G. M. Reynolds, J. R. Maxwell, and N. M. Hintz, University of Minnesota Linear Accelerator Laboratory Annual Progress Report, p. 98, 1965 (unpublished); J. R. Maxwell, G. M. Reynolds, and N. M. Hintz, University of Minnesota John H. Williams Laboratory of Nuclear Physics, p. 77, 1966 (unpublished); Claude Détraz, Joseph Cerny, and Richard H. Pehl, Phys. Rev. Letters 14, 708 (1965); J. Cerny, C. Détraz, and R. H. Pehl, Phys. Rev. 152, 950 (1966).

29. D. R. Goosman and R. W. Kavanagh, Nuclear Energy Levels of ^{37}K, April 1967 (preprint).

Table I. Energy losses of various particles in a triple-counter telescope.

Particle	E_{total} (MeV)	Energy Losses In Counters (MeV)		
		5.2 mil ΔE2 ctr	4.2 mil ΔE1 ctr	6.5 mil E ctr
^{6}He	29.00	8.27	9.17	11.56
^{3}He	21.25	6.25	7.15	7.85
d	7.75	2.53	2.94	2.28
^{3}He + d (sum)	29.00	8.78	10.09	10.13
^{8}He	35.50	8.67	8.93	17.90
^{4}He	27.50	6.18	6.24	15.08
d	8.00	2.39	2.69	2.92
^{4}He + d (sum)	35.50	8.57	8.93	18.00
^{4}He + d (sum)	35.50	8.66	9.45	17.39

Table II. Forward angle differential cross sections for four (^{3}He, ^{6}He) reactions.

Reaction	Bombarding Energy (MeV)	θ_{cm} (deg)	$d\sigma/d\Omega$ $(\mu b/sr)_{cm}$
$^{12}C(^{3}He,^{6}He)^{9}C$ g.s.	65.5	15.8	1.6 ± 0.4
$^{16}O(^{3}He,^{6}He)^{13}O$ g.s.	65.3	15.3	0.76 ± 0.12
$^{24}Mg(^{3}He,^{6}He)^{21}Mg$ g.s.	55.9	18.0	0.52 ± 0.12
$^{40}Ca(^{3}He,^{6}He)^{37}Ca$ g.s.	55.9	12.9	0.13 ± 0.03

Table III. Levels in ^{21}Na observed in the ^{23}Na(p,t)^{21}Na reaction at 42 MeV. The J^{π} assignments were all taken from the references cited.

Level Number	Excitation This Work (MeV ± keV)	Excitation Other Work (MeV ± keV)	J^{π}	References
0	0.0		$3/2^+$	18
1	0.335 ± 10	0.338 ± 3	$5/2^+$	24
2	1.71 ± 10	1.72	$(7/2^+)$	18
3	2.42 ± 30	2.430 ± 3	$1/2^+$	25
4	2.81 ± 20	2.81 ± 40		18
5	3.54 ± 20	3.540 ± 2	$5/2^+$	24
6	3.64 ± 30			
7	3.83 ± 20	3.88, 3.82		18, 24
		4.15	$3/2^-$	18, 24
8	4.28 ± 30	4.29 ± 4	$5/2^+$	24
9	4.41 ± 30	4.41 ± 20		24
		4.46 ± 5	$3/2^+$	24
10	4.99 ± 30	5.00 ± 50		18
11	5.34 ± 30			
		5.47		18
		5.70		18
12	5.78 ± 30	5.83		18
13	6.16 ± 30			
		6.26		18
14	6.54 ± 30	6.52 ± 50	$3/2^+$	18, 26
15	7.06 ± 30			
		7.21 ± 50	$1/2^+$	26

Table III. (continued)

Level Number	Excitation This Work (MeV ± keV)	Excitation Other Work (MeV ± keV)	J^{π}	References
		7.45 ± 50	$5/2^{+}$	18, 26
16	7.60 ± 60			
17	8.11 ± 30			
18	8.31 ± 30			
19	8.92 ± 30	8.90 ± 40	$(5/2^{+})$, T=3/2	19
20	9.19 ± 30			
21	10.05 ± 40			
22	11.00 ± 30			

Table IV. Isobaric multiplet mass equation predictions and calculated coefficients.

Isobaric Multiplet Mass Equation

$$M(A,T,T_z) = \underline{a}(A,T) + \underline{b}(A,T)T_z + \underline{c}(A,T)T_z^2 \quad [+ \underline{d}(A,T)T_z^3]$$

T_z=-3/2 Nucleus	Experimental Mass Excess (MeV)	Predicted Mass Excess (MeV)	$\underline{b}(A,T)$ (MeV)	$\underline{c}(A,T)$ (keV)	$[\underline{d}(A,T)]$ (keV)	$\overline{Z\alpha c}$ (keV)
^{9}C	28.99 (70)[a,b]					
^{9}C	28.916 (5)[c]	28.961 (29)	-1.332 (7)	278 (11)	7 (5)	9
^{13}O	23.11 (70)[d]	23.10 (49)	-2.180 (16)	254 (11)	-1 (14)	12
^{21}Mg	10.62 (120)	10.59 (120)	-3.545 (40)	154 (24)	-5 (28)	12
^{37}Ca	-13.24 (50)	-13.24 (118)	-6.176 (39)	176 (25)	1 (21)	24

[a] All errors are in parentheses and are in keV.

[b] See Ref. 5.

[c] See Ref. 6.

[d] See Ref. 7.

Table V. Comparison between various systematic mass predictions and the experimental masses.

Nucleus	Experimental Mass Excess[a] (MeV)	Goldansky[b] Mass Excess (MeV)	Jänecke[c] Mass Excess (MeV)	Kelson-Garvey[d] Mass Excess (MeV)
^{9}C	28.916 (5)[e]	-	29.3	28.88
^{13}O	23.11 (70)[f]	23.2	23.4	23.52
^{21}Mg	10.62 (120)	10.9	10.8	10.79
^{37}Ca	-13.24 (50)	-12.9	-	-13.17

[a] Values in parentheses are the mass excess errors in keV.

[b] See Ref. 1.

[c] See Ref. 2.

[d] See Ref. 3.

[e] See Ref. 6.

[f] See Ref. 7.

FIGURE CAPTIONS

Fig. 1. Schematic diagram of the cyclotron facility and the relevant beam optics and equipment.

Fig. 2. Schematic diagram of the electronic setup when employing the standard particle-identifier system; it presents one of the two independent counter telescopes.

Fig. 3. Standard particle-identifier spectrum from the bombardment of a sodium target with 42-MeV protons. The ΔE counter thickness was 5.6 mils.

Fig. 4. Schematic diagram of the electronics for the triple-counter particle-identification system.

Fig. 5. Simplified illustration of the function of the triple-counter particle identifier.

Fig. 6. Standard particle identifier spectra from the bombardment of a ^{12}C target with 70-MeV ^{4}He ions (open circles) and with 65-MeV ^{3}He ions (filled circles). The ΔE and E detector thicknesses were 8.5 mils and 120 mils, respectively.

Fig. 7. A ^{6}He energy spectrum from the $^{12}C(^{3}He,^{6}He)^{9}C$ reaction at 65 MeV. This reaction was investigated using a standard particle-identifier system.

Fig. 8. Triple-counter particle-identifier spectrum from ^{12}C + 65-MeV ^{3}He-particles. The $\Delta E2$, $\Delta E1$ and E detector thicknesses were 5.2 mils, 4.2 mils, and 5.6 mils, respectively.

Fig. 9. Energy spectrum of the $^{12}C(^{3}He,^{6}He)^{9}C$ reaction at 65 MeV; the counts due to the $^{16}O(^{3}He,^{6}He)^{13}O$ reaction resulted from the oxygen in the Mylar target. These results were obtained using the triple-counter particle-identification system.

Fig. 10. Pulser-simulated particle-identifier spectra for the triple-counter system using the detector thicknesses shown in Fig. 4; (c) shows the normal positions of the particle-stable nuclei from ^{3}He to ^{7}Li, while (a) and (b) show the positions of $^{4}He + X$ and $^{3}He + X$ (X denotes p, d, t, ^{3}He, or ^{4}He) chance coincidences, respectively.

Fig. 11. Time plots of (a) the ^{3}He beam energy as determined by elastic scattering in the monitor detector and (b) the electronic drifts in the E_{total} pulse of one triple-counter ^{6}He detection system during a study of the $^{40}Ca(^{3}He,^{6}He)^{37}Ca$ reaction.

Fig. 12. Triple-counter particle-identifier spectrum from 55.9-MeV ^{3}He ions incident on a ^{40}Ca target.

Fig. 13. Plots of $\Delta E2$ and $\Delta E1$ versus E_{total} for the events in the ^{6}He region of the particle-identifier spectrum during the $^{40}Ca(^{3}He,^{6}He)^{37}Ca$ experiment.

Fig. 14. Energy spectra from (a) the $^{24}Mg(^{3}He,^{6}Li)^{21}Na$ reaction and (b) the $^{40}Ca(^{3}He,^{6}Li)^{37}K$ reaction at 55.9 MeV.

Fig. 15. Triple-counter particle-identifier spectrum resulting from the bombardment of ^{24}Mg with 55.9-MeV ^{3}He ions.

Fig. 16. Two independent ^{6}He energy spectra from the $^{24}Mg(^{3}He,^{6}He)^{21}Mg$ reaction at 55.9 MeV and a scattering angle of 14.1 deg. Each block represents one count and the block width is 100 keV.

Fig. 17. Two independent ^{6}He energy spectra from the $^{40}Ca(^{3}He,^{6}He)^{37}Ca$ reaction at 55.9 MeV; the data from both systems were kinematically corrected to 11.2 deg. Each block is one count and the block width is 100 keV.

Fig. 18. Energy spectra from the $^{22}Ne(d,t)^{21}Ne$ and $^{22}Ne(d,^{3}He)^{21}F$ reactions at 20.5 deg. The ^{21}Ne spectrum has been adjusted to align the first three T = 3/2 levels in ^{21}Ne with their analogues in the ^{21}F spectrum.

Fig. 19. Angular distributions of the $^{22}Ne(d,t)^{21}Ne$ transitions to the ground state ($3/2^+$), 0.35-MeV ($5/2^+$) and 8.92-MeV levels and of the $^{22}Ne(d,^3He)^{21}F$ ground-state ($5/2^+$) transition. In all cases smooth curves have been drawn through the experimental points to guide the eye; the abscissa is the dimensionless quantity QR, where Q is the momentum transfer and R is the interaction radius.

Fig. 20. Angular distributions for the $^{22}Ne(d,^3He)^{21}F^*$ 0.28-MeV ($1/2^+$) and the $^{22}Ne(d,t)^{21}Ne^*$ 9.21-MeV transitions.

Fig. 21. Angular distributions of the $^{16}O(d,^3He)^{15}N$ ground-state ($1/2^-$) and 6.33-MeV ($3/2^-$) transitions, the $^{22}Ne(d,^3He)^{21}F^*$ 1.10-MeV transition and the $^{22}Ne(d,t)^{21}Ne^*$ 10.04-MeV transition.

Fig. 22. Triton energy spectrum from the $^{23}Na(p,t)^{21}Na$ reaction at 42 MeV. The numbered levels are ^{21}Na levels whose average excitation energies are listed in Table III.

Fig. 23. Energy level diagrams for the members of the mass 21 isospin quartet showing the positions of the $T = 3/2$ levels in each nucleus. For the sake of clarity the ground-state energies of mirror nuclei have been equated and many of the excited levels of ^{21}Ne and ^{21}Na below 10 MeV excitation have been deleted.

Fig. 24. Energy spectra from the $^{39}K(p,^3He)^{37}Ar$ and $^{39}K(p,t)^{37}K$ reactions at 45 MeV and a scattering angle of 26 deg. The spectra have been adjusted to align the positions of the ground-state peaks.

Fig. 25. Relative angular distributions for the $^{39}K(p,t)^{37}K$ ground-($3/2^+$), 1.37-MeV ($1/2^+$), and 5.035-MeV ($T = 3/2$) states and for the $^{39}K(p,^3He)^{37}Ar^*$ 5.010-MeV ($T = 3/2$) state. The cross section of the last transition has been corrected for phase space and isospin coupling factors.

Fig. 26. Energy level diagrams of the members of the mass 37 isospin quartet showing the positions of the T = 3/2 levels in each nucleus. For clarity the ground-state masses of mirror nuclei have been equated and several of the ^{37}Ar and ^{37}K energy levels have been deleted.

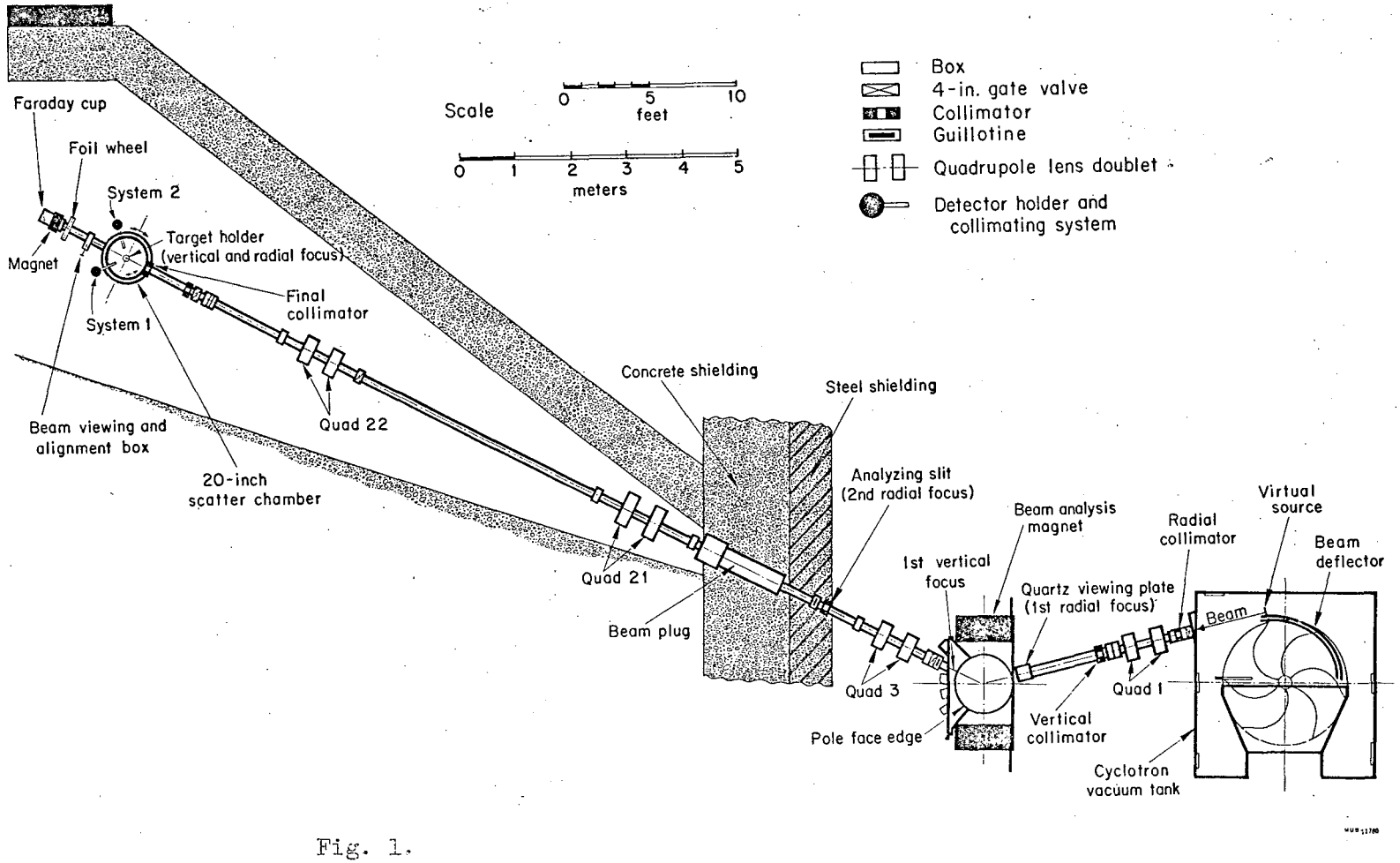
Faraday cup
Foil wheel
System 2
Target holder
(vertical and radial focus)
Magnet
System 1
Final
collimator
Beam viewing and
alignment box
20-inch
scatter chamber
Quad 22
Quad 21
Beam plug
Concrete shielding
Steel shielding
Analyzing slit
(2nd radial focus)
Beam analysis
magnet
1st vertical
focus
Quartz viewing plate
(1st radial focus)
Radial
collimator
Virtual
source
Beam
deflector
Beam
Quad 3
Quad 1
Pole face edge
Vertical
collimator
Cyclotron
vacuum tank
Scale
0 5 10
feet
0 1 2 3 4 5
meters
Box
4-in. gate valve
Collimator
Guillotine
Quadrupole lens doublet
Detector holder and
collimating system

Fig. 1.

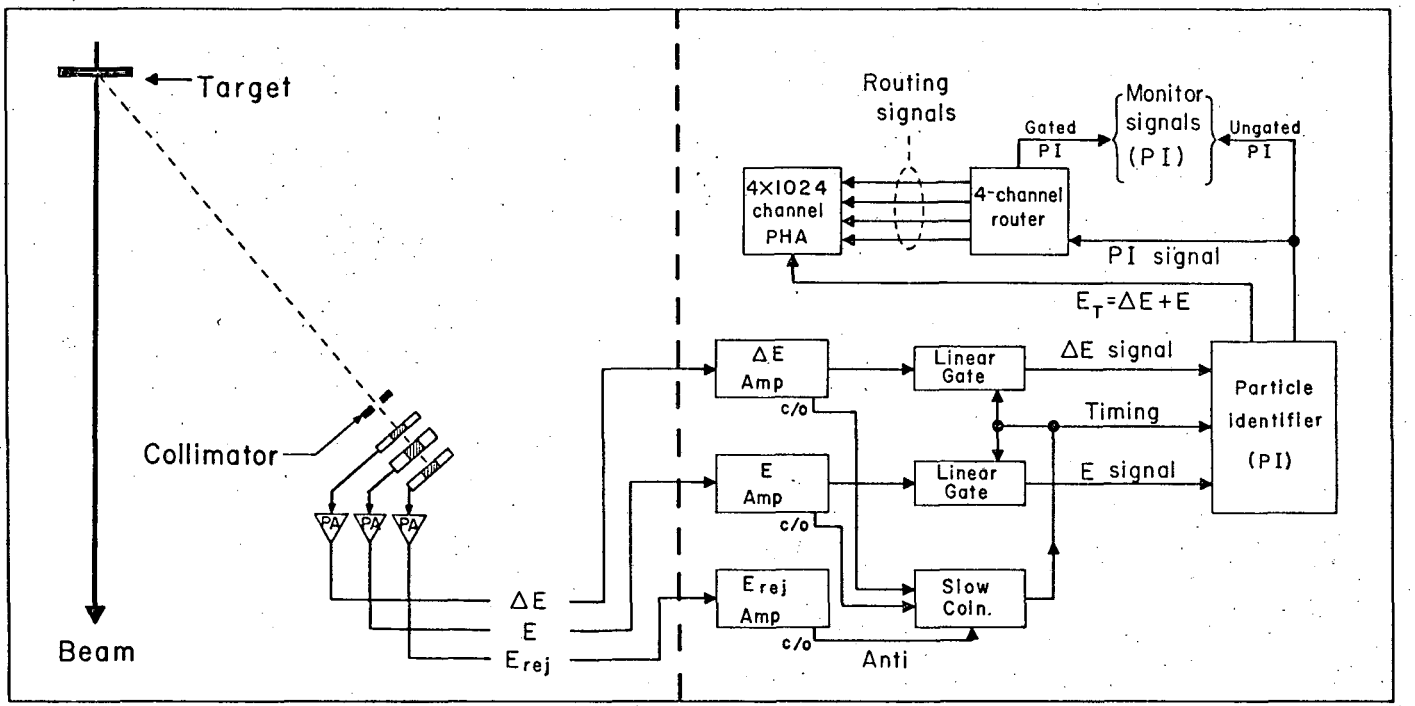

XBL676-3229-B

Fig. 2.

UCRL-17693

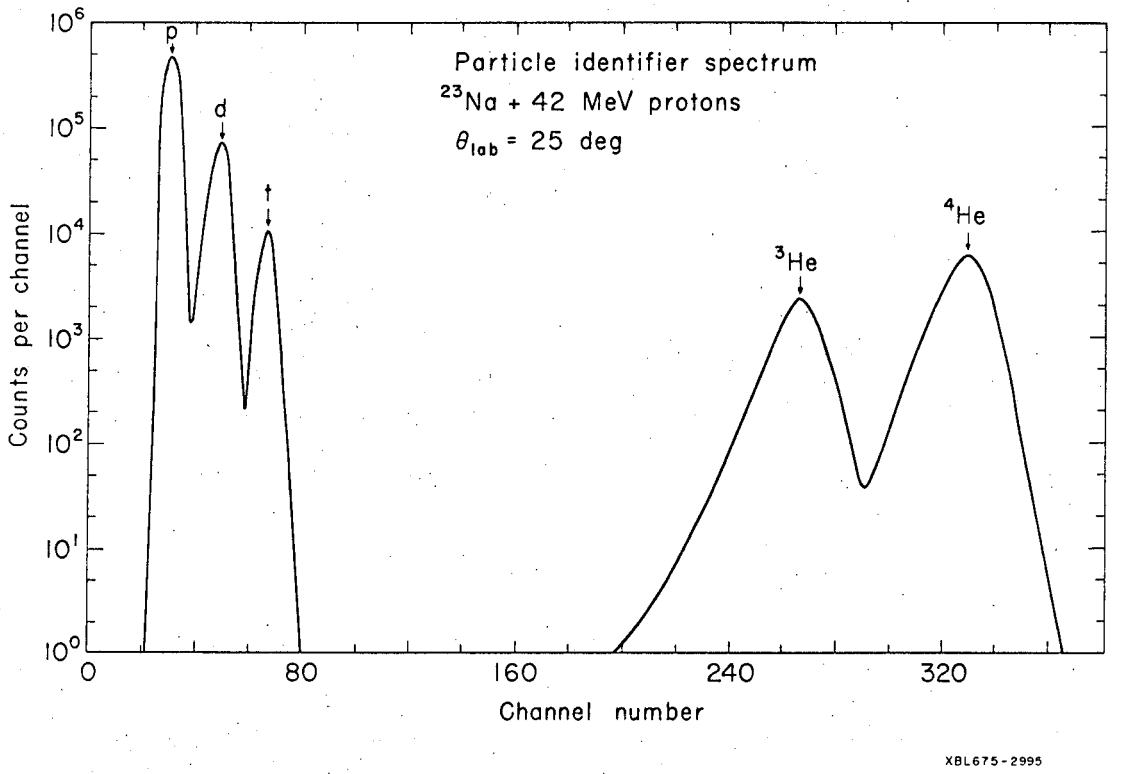
Particle identifier spectrum
^{23}Na + 42 MeV protons
θ_{lab} = 25 deg
p
d
t
^{3}He
^{4}He
Counts per channel
Channel number
10^{6}
10^{5}
10^{4}
10^{3}
10^{2}
10^{1}
10^{0}
0
80
160
240
320
XBL675-2995

Fig. 3.

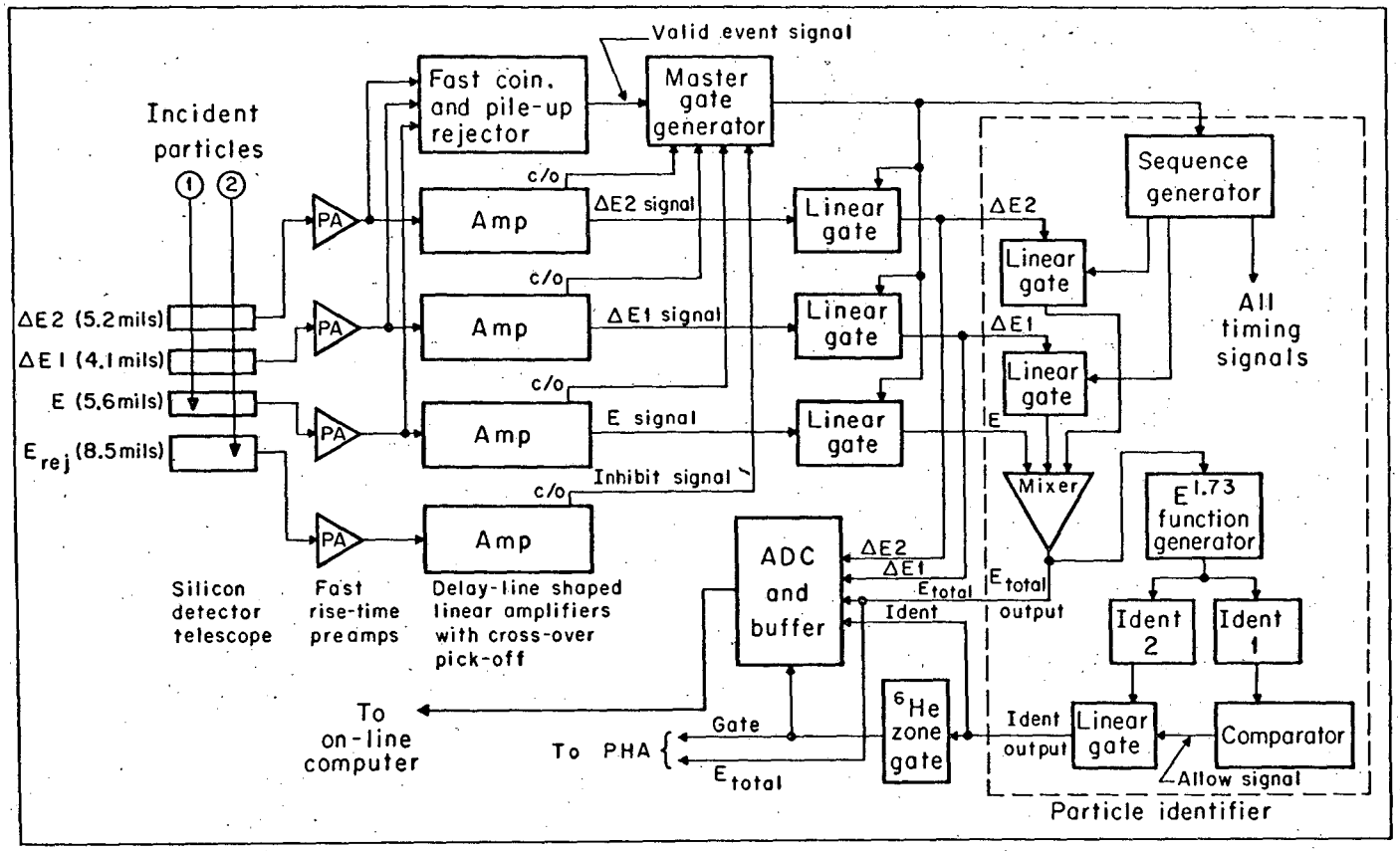

Fig. 4.

MUB-9482-A

Three counter particle identifier

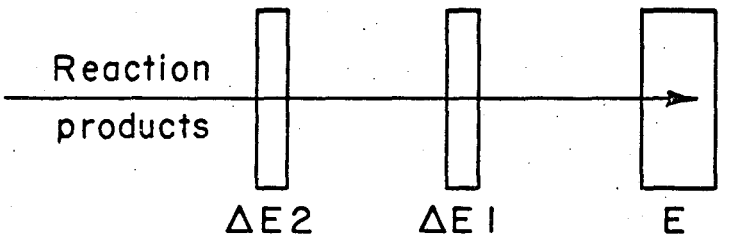

Different identification modes of the particle identifier

	ctr(s) used as "ΔE" ctr	ctr(s) used as "E" ctr
A.	ΔE2	ΔE1 + E
B.	ΔE1	E

if the ratio A/B is within a chosen percentage, then the final output is C

C.	ΔE2 + ΔE1	E

Fig. 5.

MUB-9885

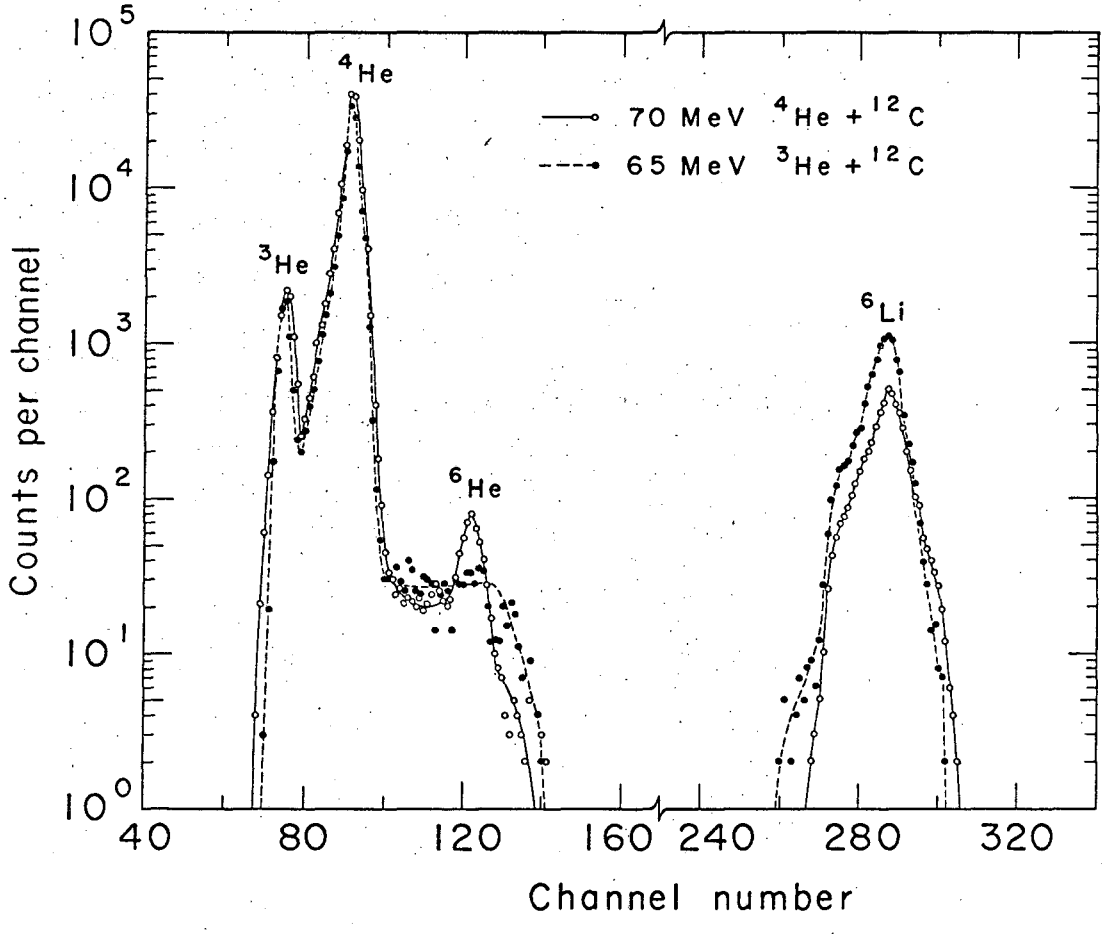
Counts per channel
Channel number
70 MeV ^{4}He + ^{12}C
65 MeV ^{3}He + ^{12}C
^{3}He
^{4}He
^{6}He
^{6}Li
10^5
10^4
10^3
10^2
10^1
10^0
40
80
120
160
240
280
320
XBL676-3339

Fig. 6.

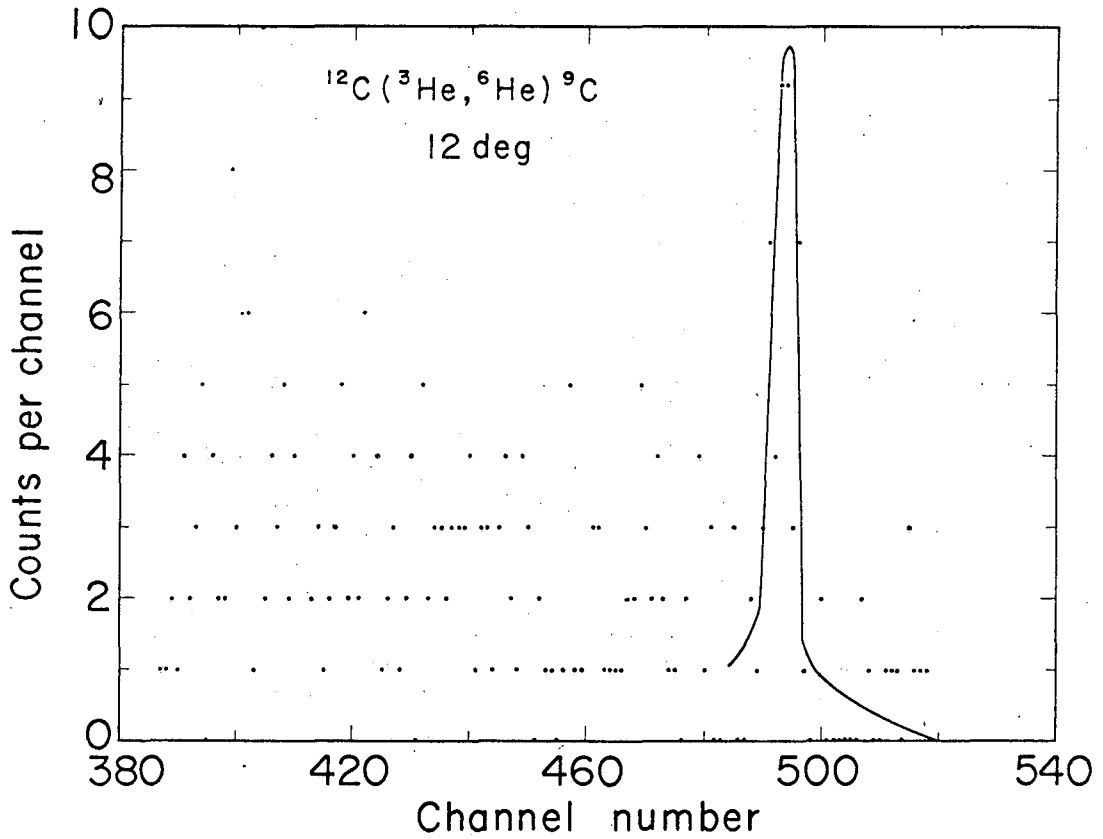

Fig. 7.

MUB-4506 A

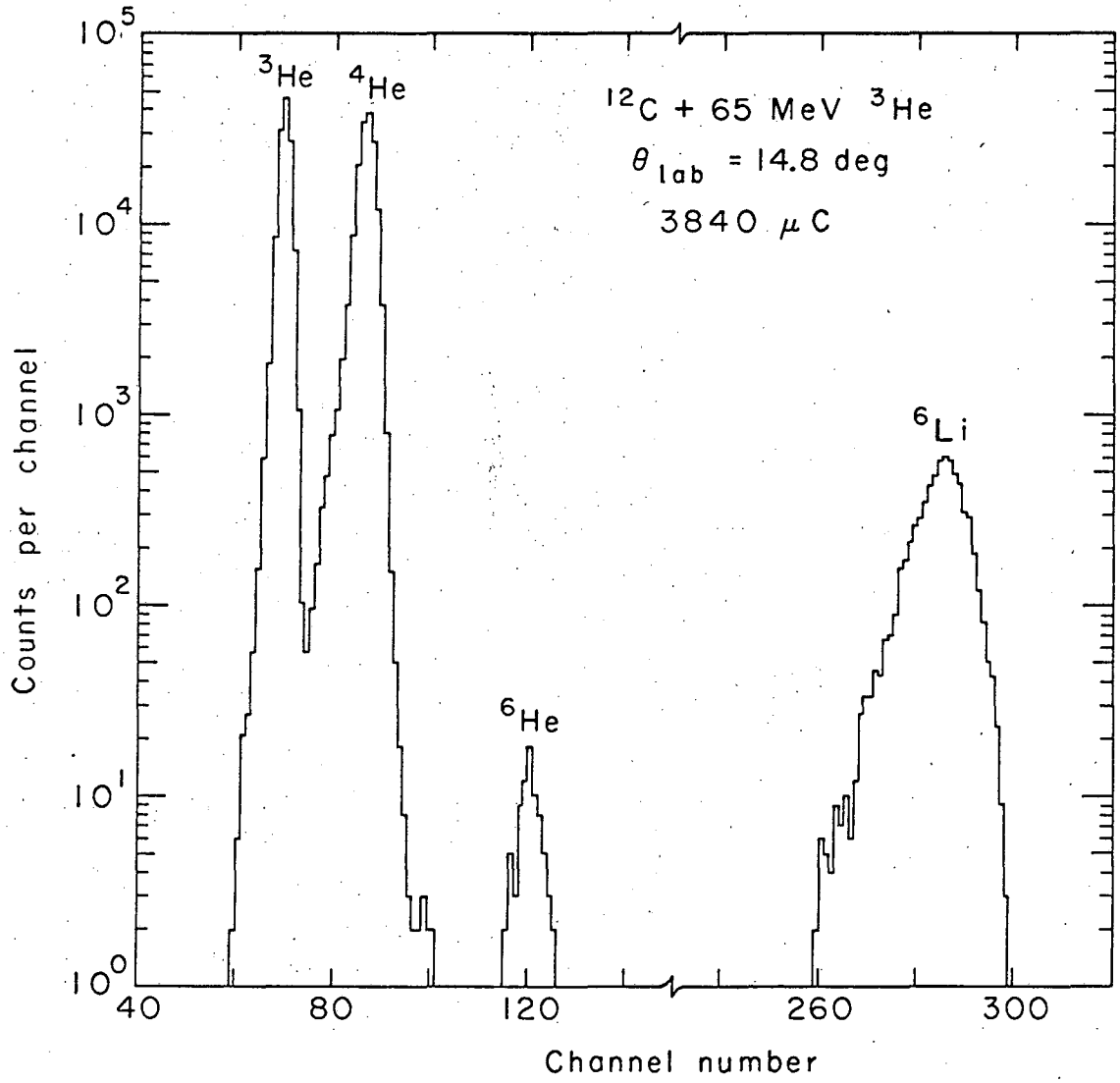
10^5
10^4
10^3
10^2
10^1
10^0
Counts per channel
^{3}He
^{4}He
^{6}He
^{6}Li
^{12}C + 65 MeV ^{3}He
θ_{lab} = 14.8 deg
3840 μC
40
80
120
260
300
Channel number
XBL676-3340

Fig. 8.

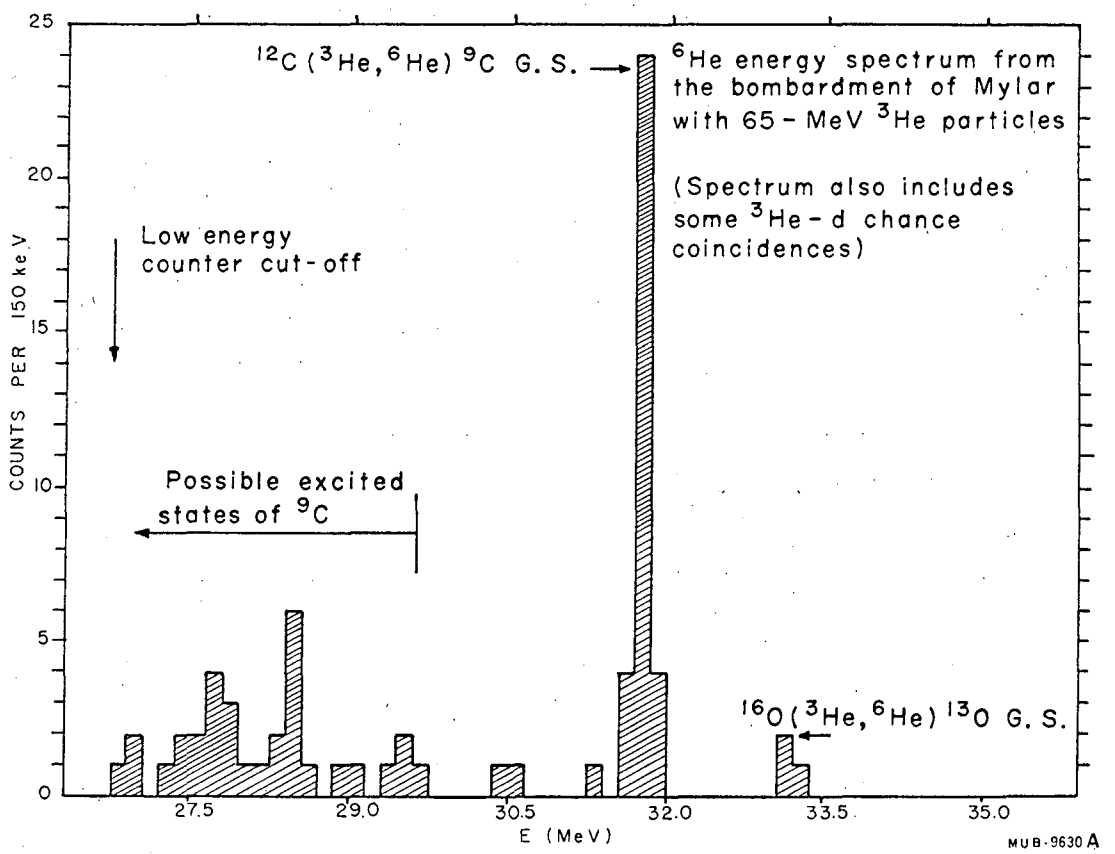
$^{12}C(^{3}He,^{6}He)^{9}C$ G.S.
^{6}He energy spectrum from the bombardment of Mylar with 65 - MeV ^{3}He particles
(Spectrum also includes some ^{3}He - d chance coincidences)
Low energy counter cut-off
Possible excited states of ^{9}C
$^{16}O(^{3}He,^{6}He)^{13}O$ G.S.
COUNTS PER 150 keV
E (MeV)
MUB-9630A

Fig. 9.

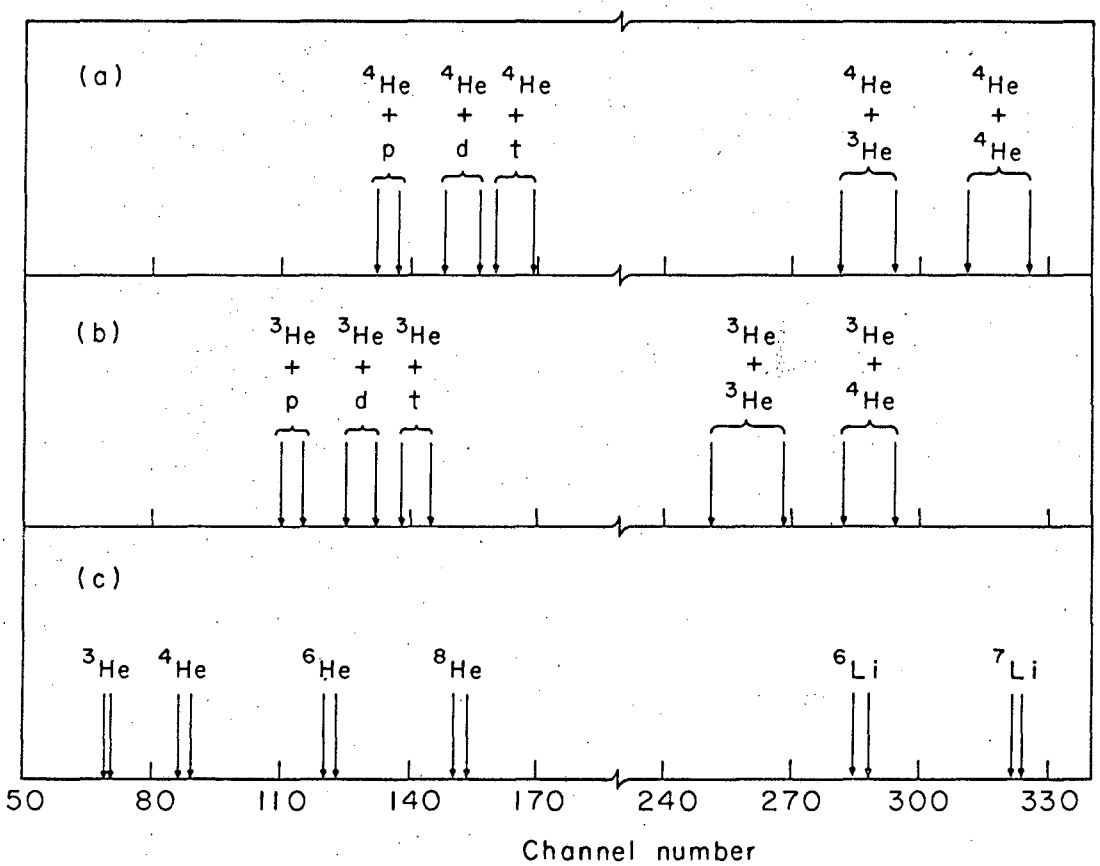

Fig. 10.

XBL676-3336

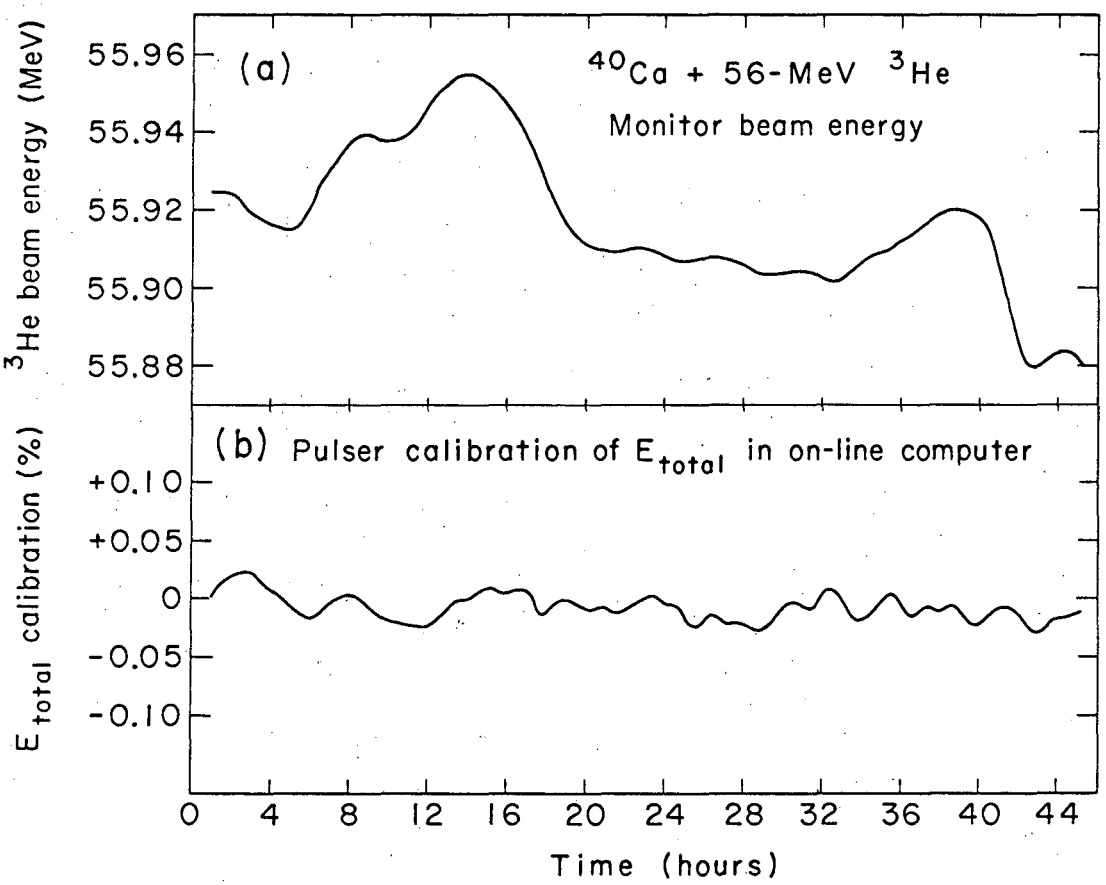

Fig. 11.

XBL676-3338

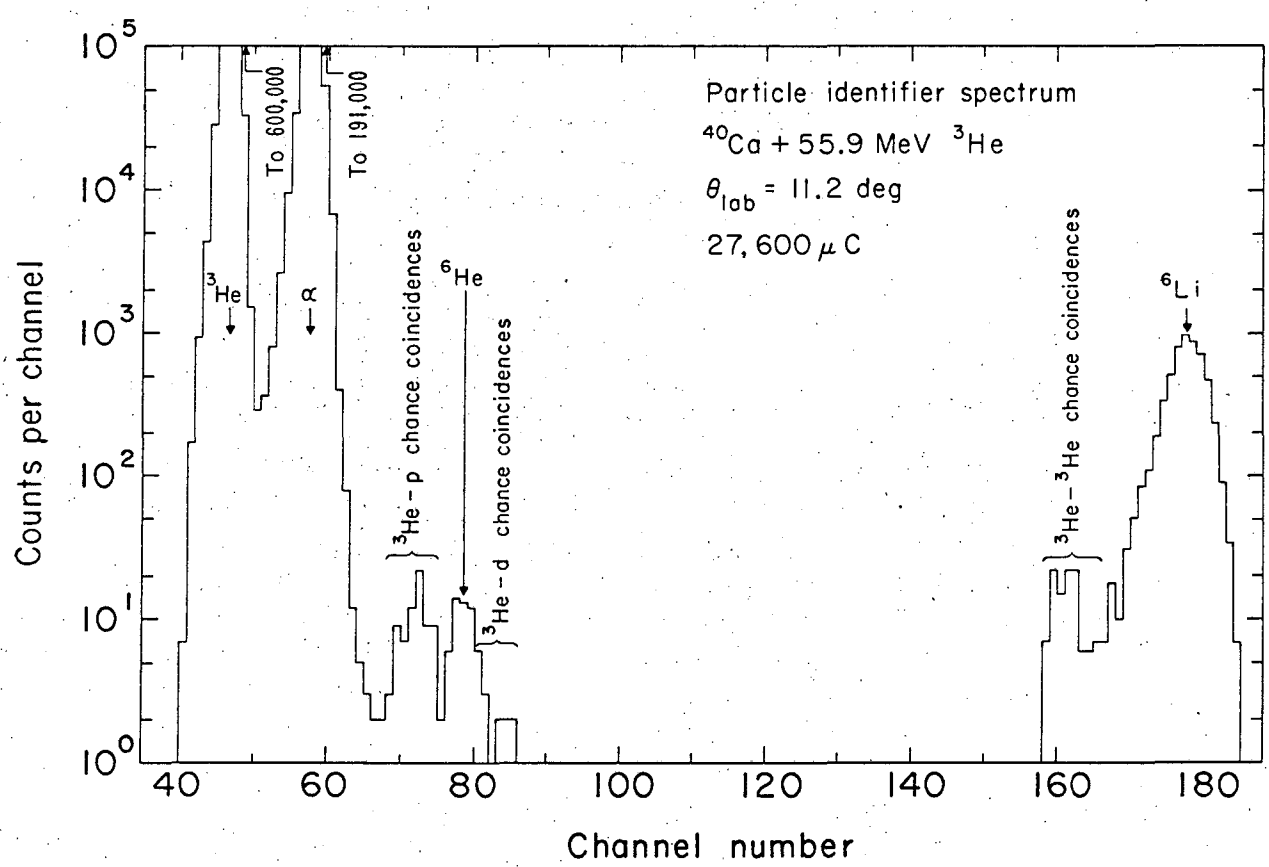

Fig. 12.

MUB-9799

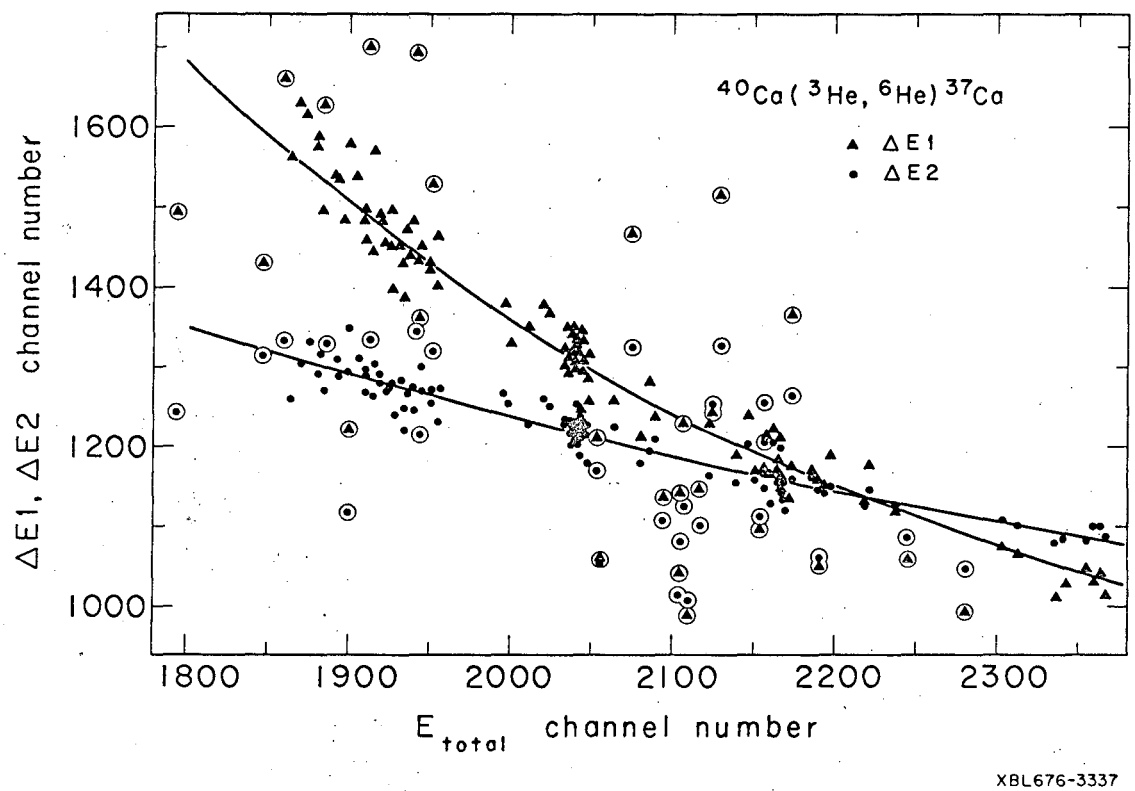
$^{40}Ca(^{3}He, ^{6}He)^{37}Ca$
▲ ΔE1
• ΔE2
ΔE1, ΔE2 channel number
1600
1400
1200
1000
1800
1900
2000
2100
2200
2300
E_{total} channel number
XBL676-3337

Fig. 13.

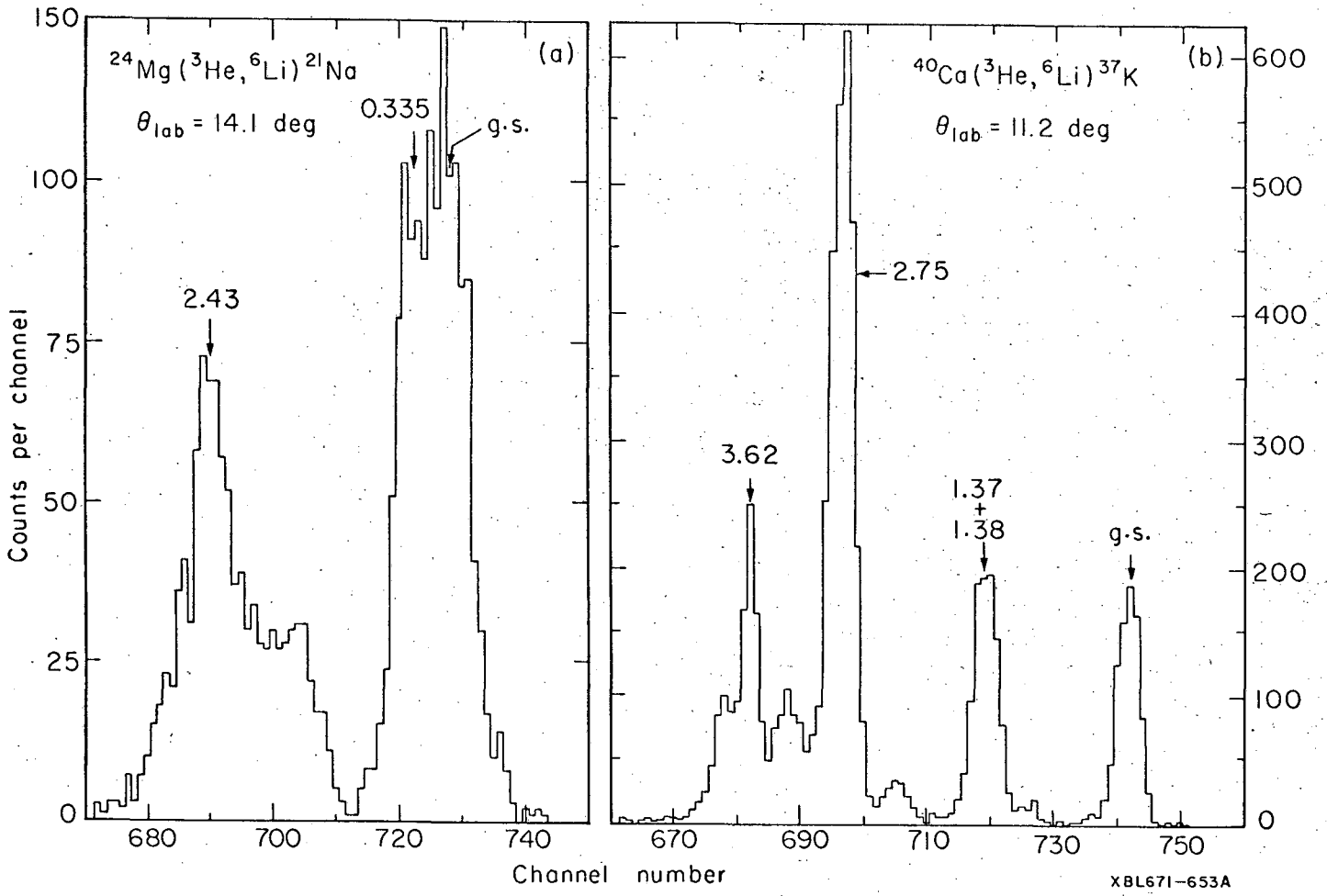
^{24}Mg(^{3}He,^{6}Li)^{21}Na
(a)
θ_{lab} = 14.1 deg
0.335
g.s.
2.43
^{40}Ca(^{3}He,^{6}Li)^{37}K
(b)
θ_{lab} = 11.2 deg
2.75
3.62
1.37
+
1.38
g.s.
Counts per channel
Channel number
XBL671-653A

Fig. 14.

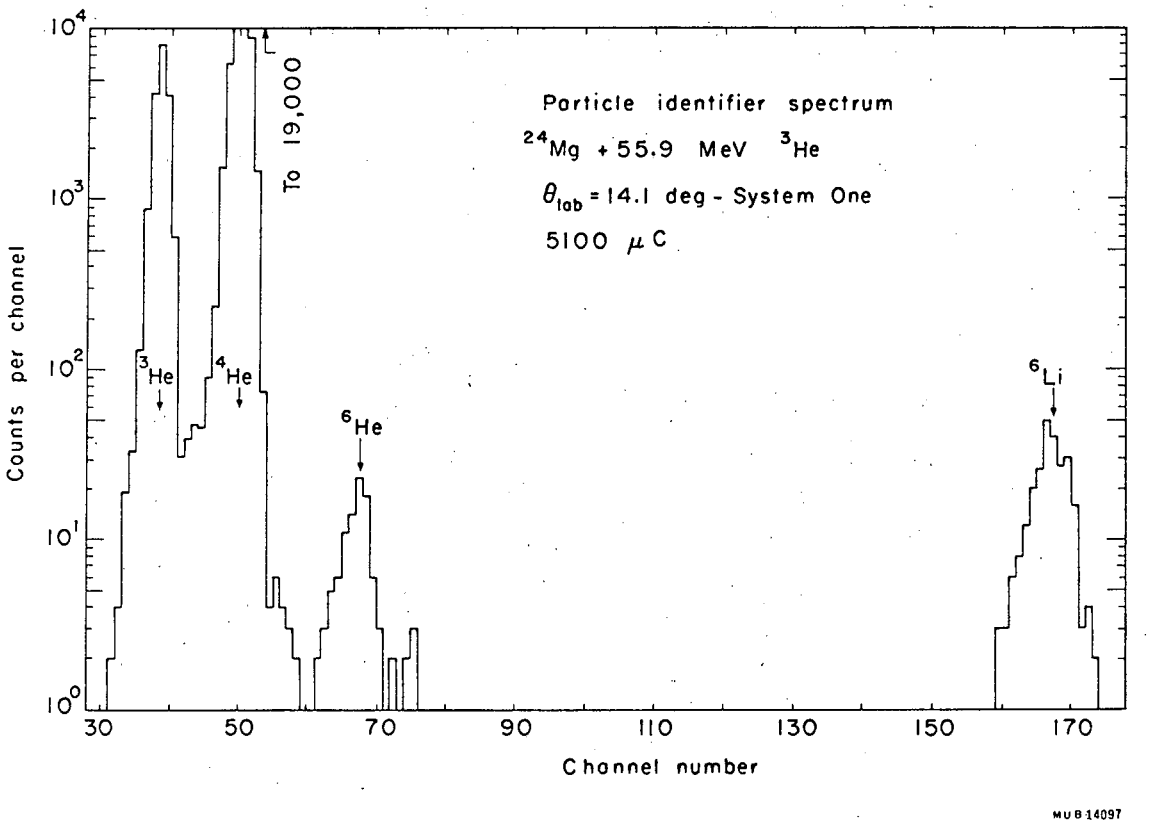
Particle identifier spectrum
^{24}Mg + 55.9 MeV ^{3}He
θ_{lab} = 14.1 deg - System One
5100 μC
To 19,000
^{3}He
^{4}He
^{6}He
^{6}Li
Counts per channel
Channel number
MUB-14097

Fig. 15.

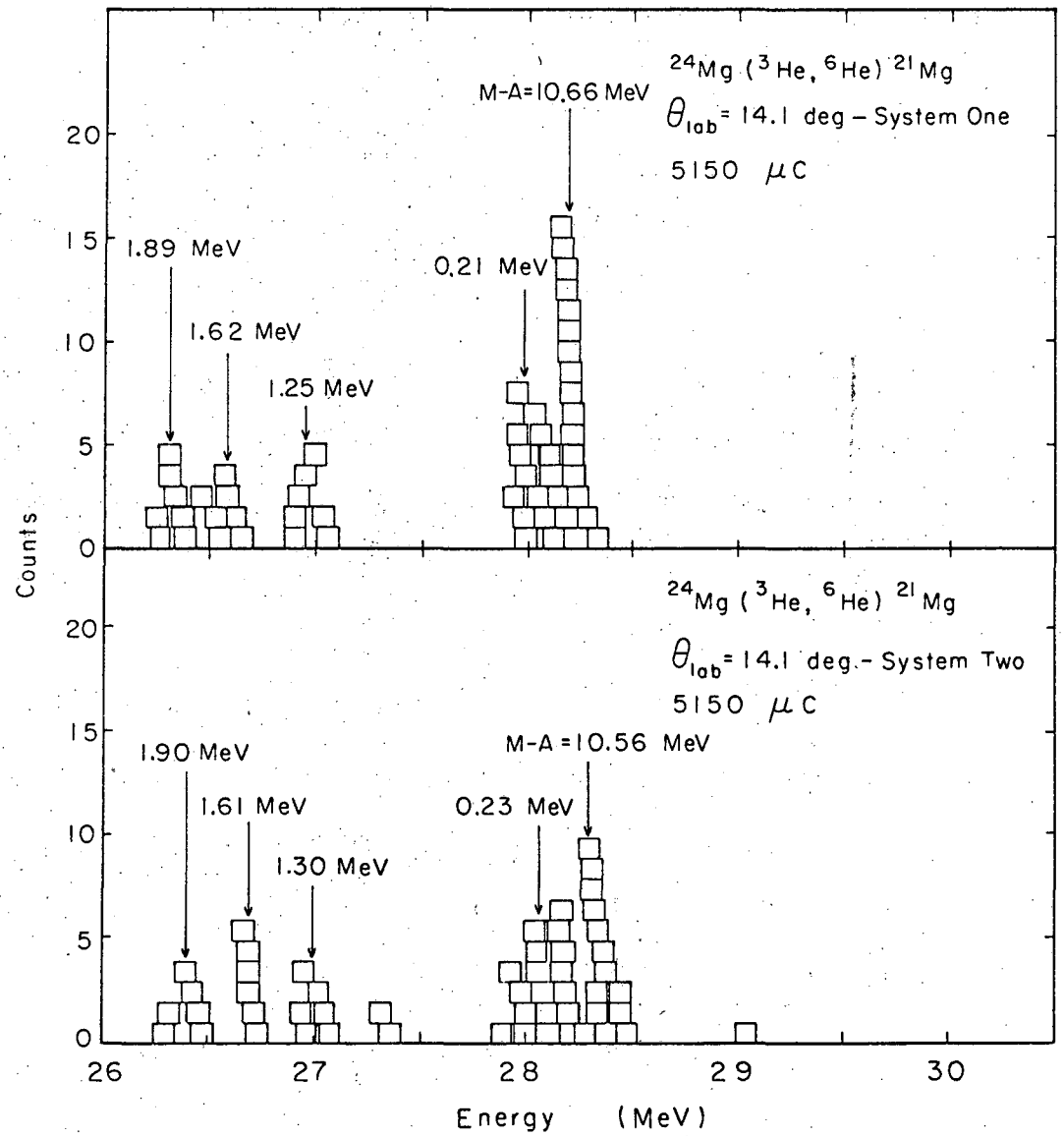
^{24}Mg (^{3}He, ^{6}He) ^{21}Mg
M-A=10.66 MeV
θ_{lab}= 14.1 deg – System One
5150 μC
1.89 MeV
1.62 MeV
1.25 MeV
0.21 MeV
^{24}Mg (^{3}He, ^{6}He) ^{21}Mg
θ_{lab}= 14.1 deg.- System Two
5150 μC
1.90 MeV
1.61 MeV
1.30 MeV
M-A = 10.56 MeV
0.23 MeV
Counts
Energy (MeV)
MUB-14099

Fig. 16.

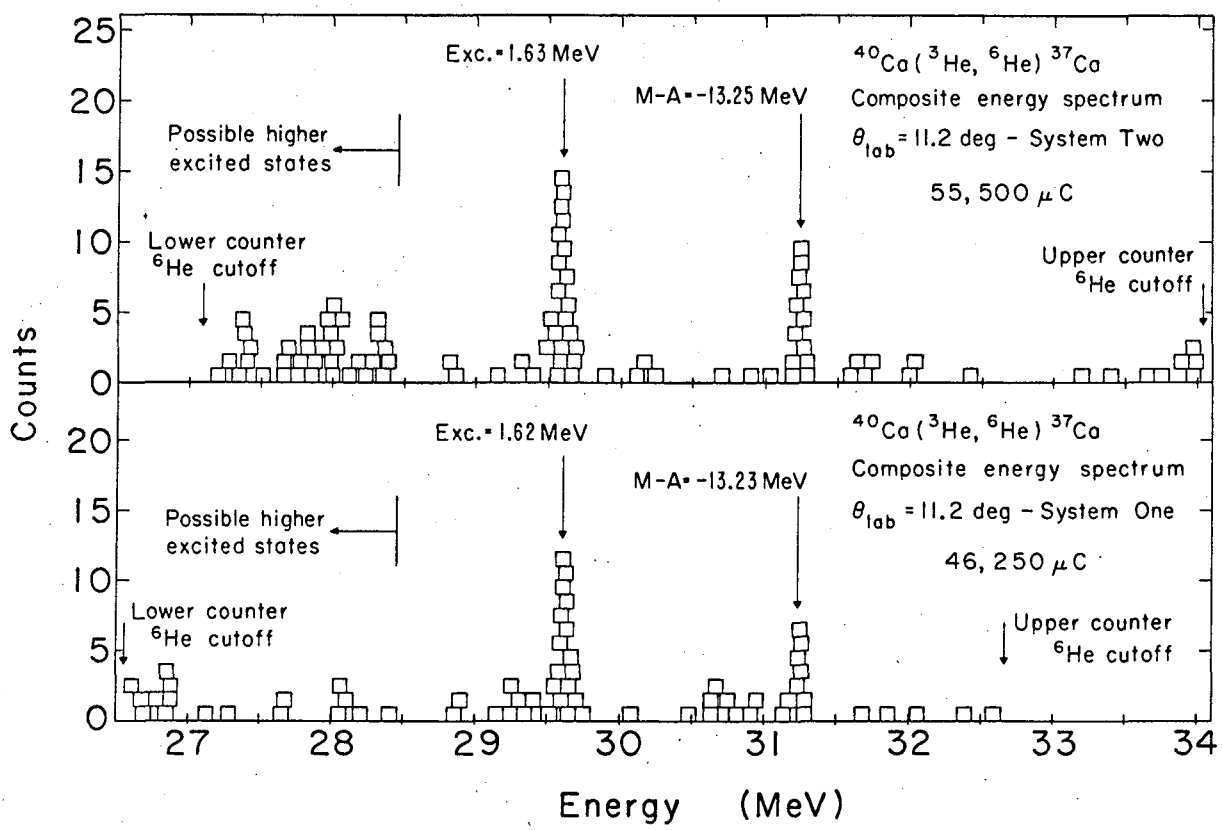
Exc.= 1.63 MeV
M-A= -13.25 MeV
^{40}Ca (^{3}He, ^{6}He) ^{37}Ca
Composite energy spectrum
θ_{lab} = 11.2 deg - System Two
55, 500 μC
Possible higher excited states
Lower counter ^{6}He cutoff
Upper counter ^{6}He cutoff
Exc.= 1.62 MeV
M-A= -13.23 MeV
^{40}Ca (^{3}He, ^{6}He) ^{37}Ca
Composite energy spectrum
θ_{lab} = 11.2 deg - System One
46, 250 μC
Possible higher excited states
Lower counter ^{6}He cutoff
Upper counter ^{6}He cutoff
Counts
Energy (MeV)
MUB-9797

Fig. 17.

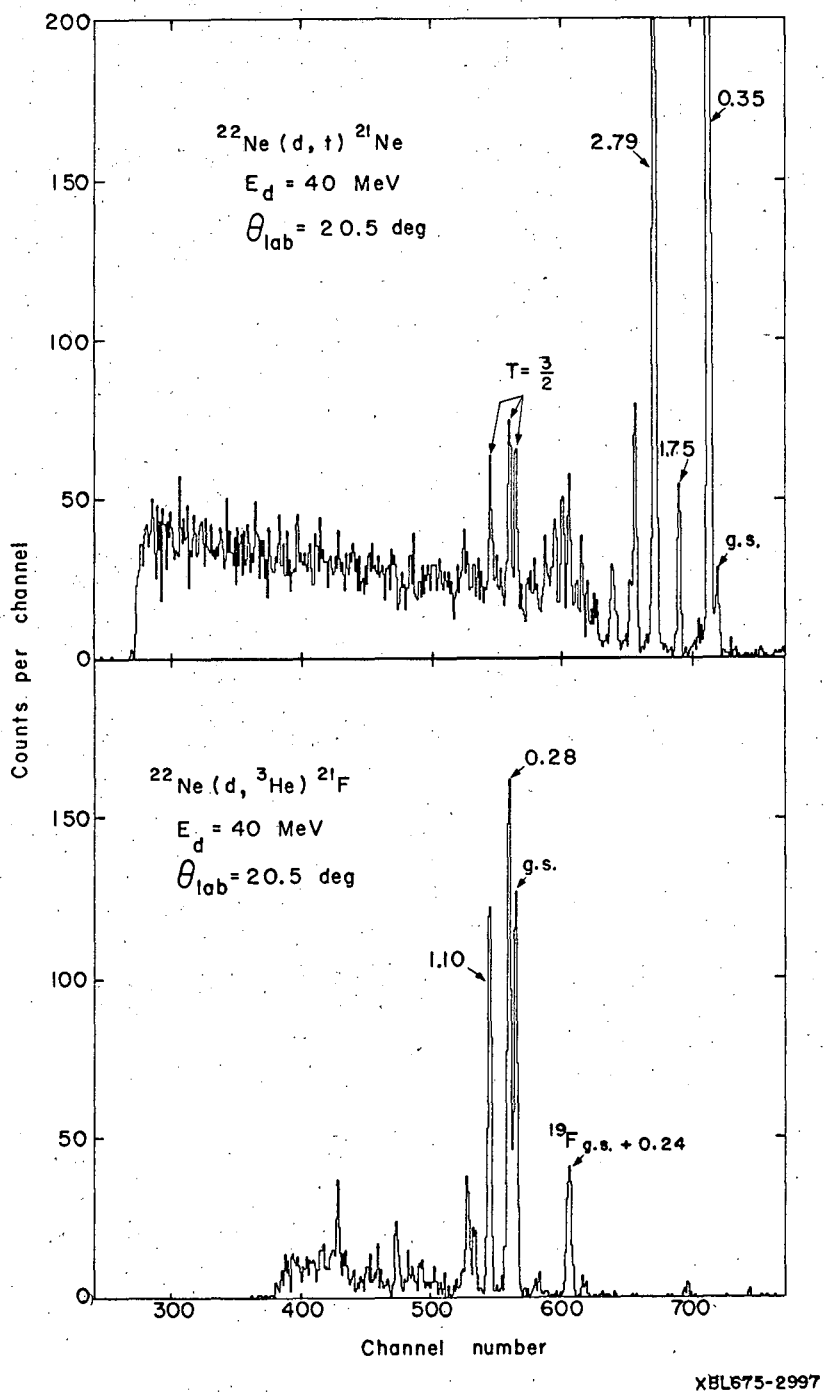
^{22}Ne (d, t) ^{21}Ne
E_d = 40 MeV
θ_{lab} = 20.5 deg
2.79
0.35
T= 3/2
1.75
g.s.
^{22}Ne (d, ^{3}He) ^{21}F
E_d = 40 MeV
θ_{lab} = 20.5 deg
0.28
g.s.
1.10
^{19}F g.s. + 0.24
Counts per channel
Channel number
0
50
100
150
200
300
400
500
600
700
XBL675-2997

Fig. 18.

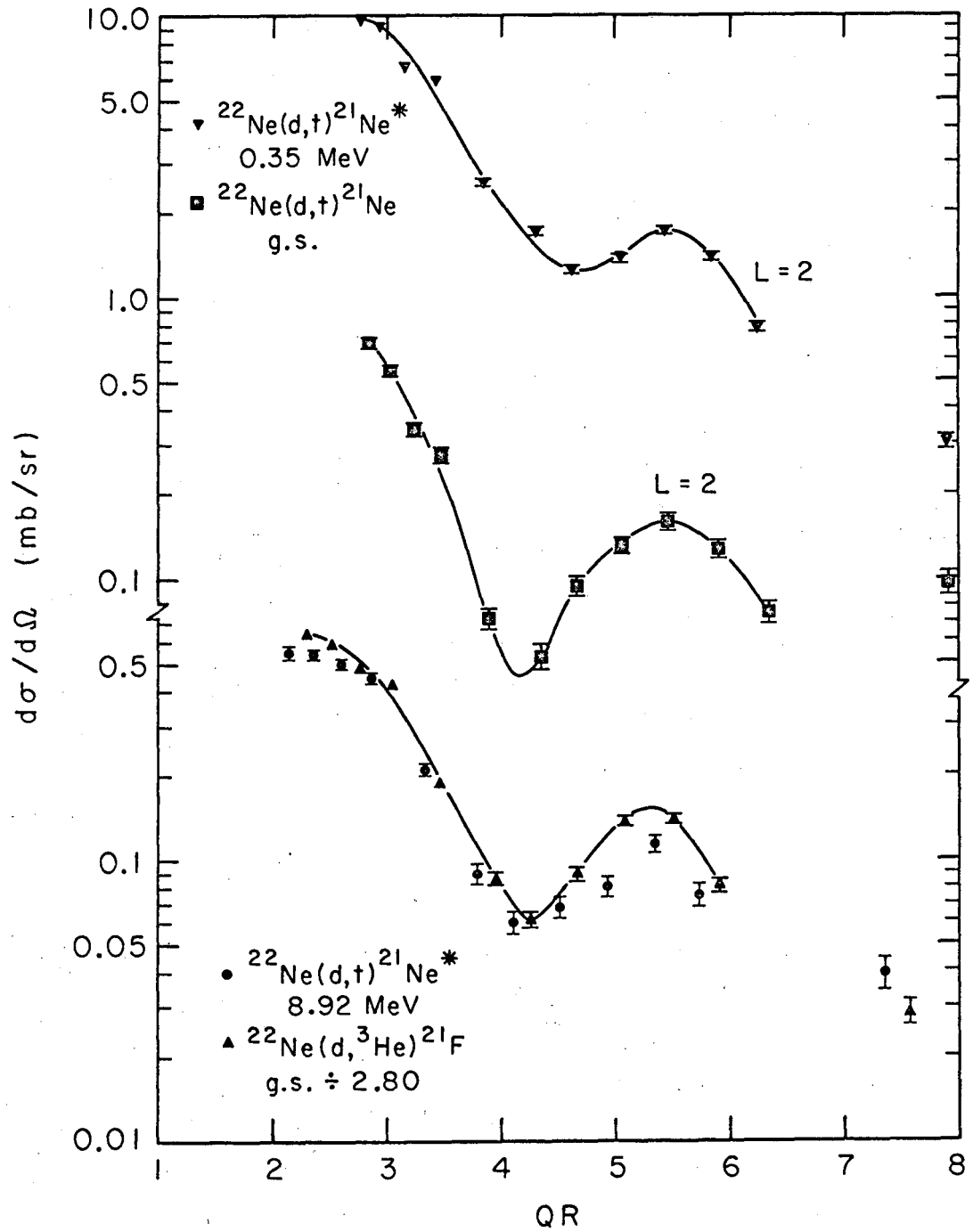
10.0
5.0
1.0
0.5
0.1
0.5
0.1
0.05
0.01
dσ/dΩ (mb/sr)
22Ne(d,t)21Ne*
0.35 MeV
22Ne(d,t)21Ne
g.s.
L = 2
L = 2
22Ne(d,t)21Ne*
8.92 MeV
22Ne(d,3He)21F
g.s. ÷ 2.80
1
2
3
4
5
6
7
8
QR
XBL677-3534

Fig. 19.

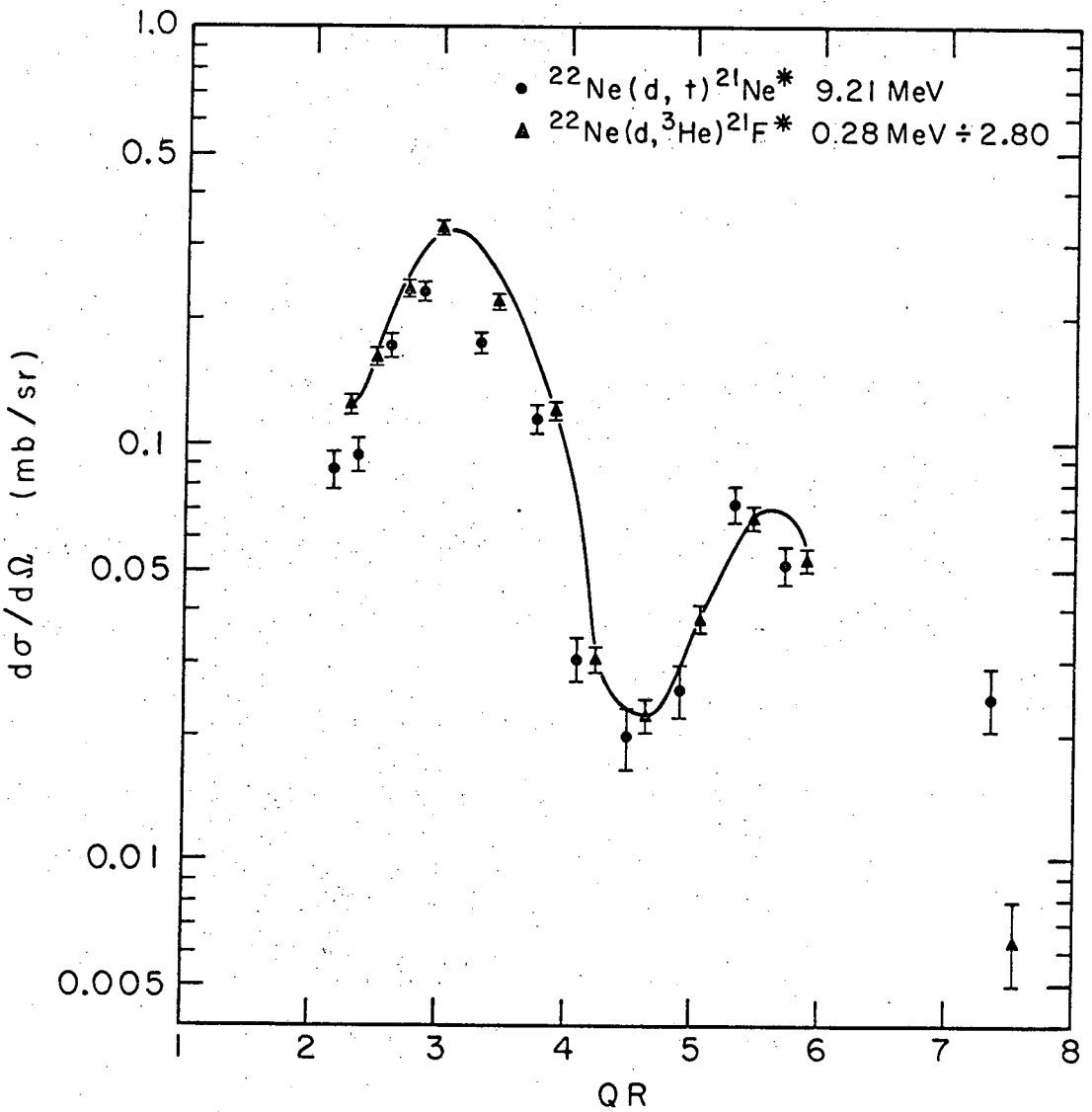

Fig. 20.

XBL677-3533

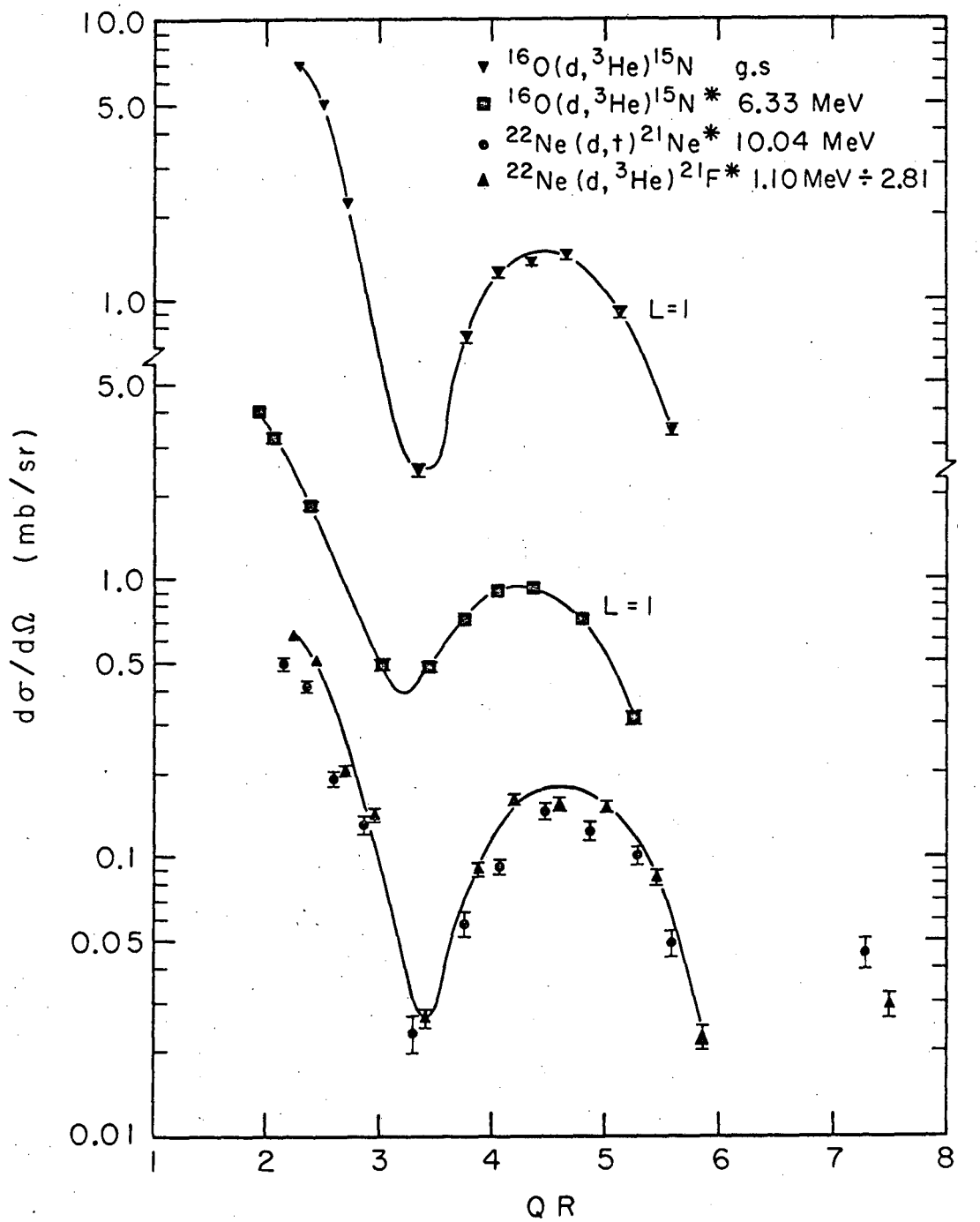

Fig. 21.

XBL677-3535

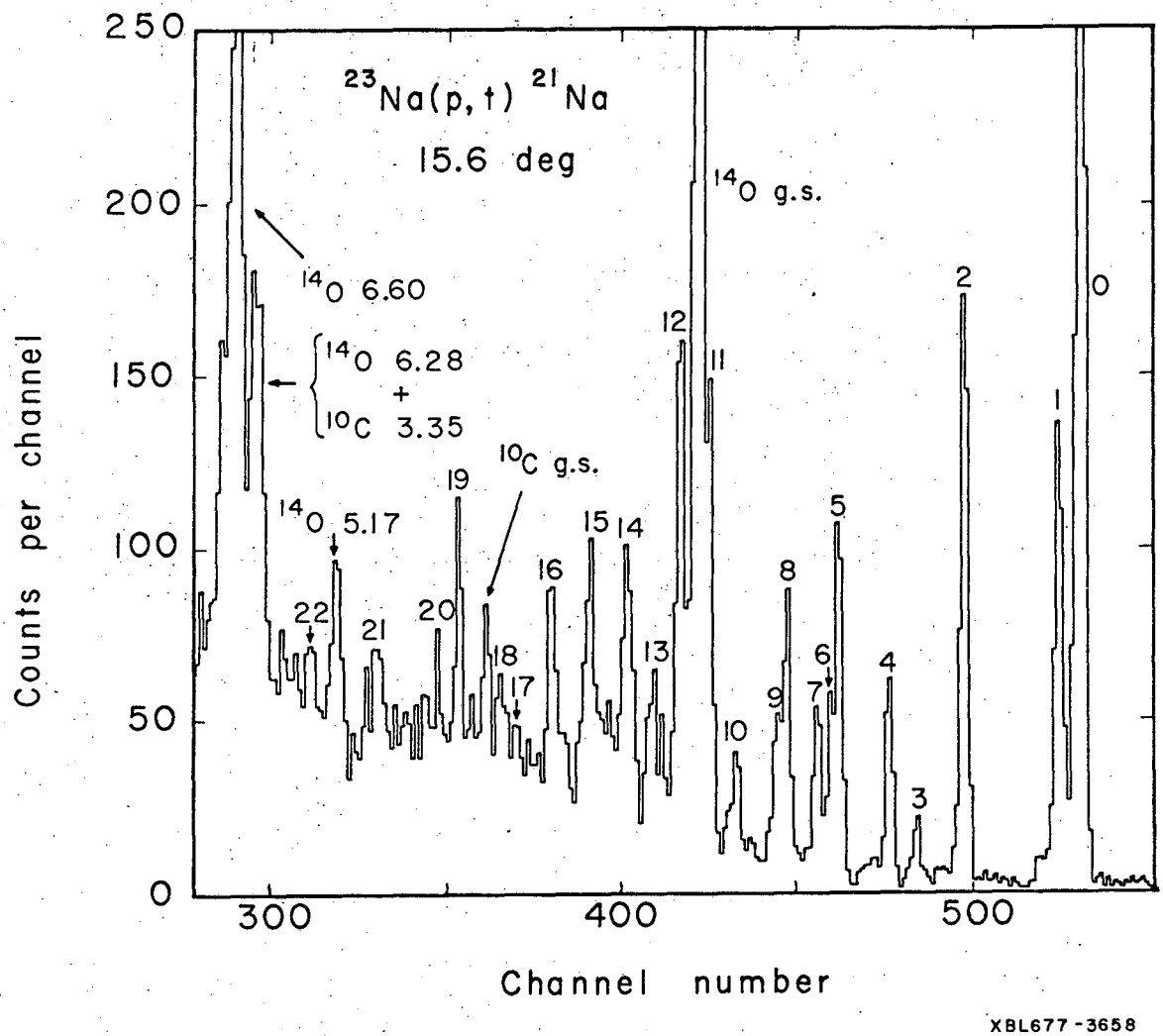
^{23}Na(p, t) ^{21}Na
15.6 deg
^{14}O g.s.
^{14}O 6.60
^{14}O 6.28
+
^{10}C 3.35
^{10}C g.s.
^{14}O 5.17
Counts per channel
Channel number
250
200
150
100
50
0
300
400
500
0
1
2
3
4
5
6
7
8
9
10
11
12
13
14
15
16
17
18
19
20
21
22
XBL677-3658

Fig. 22.

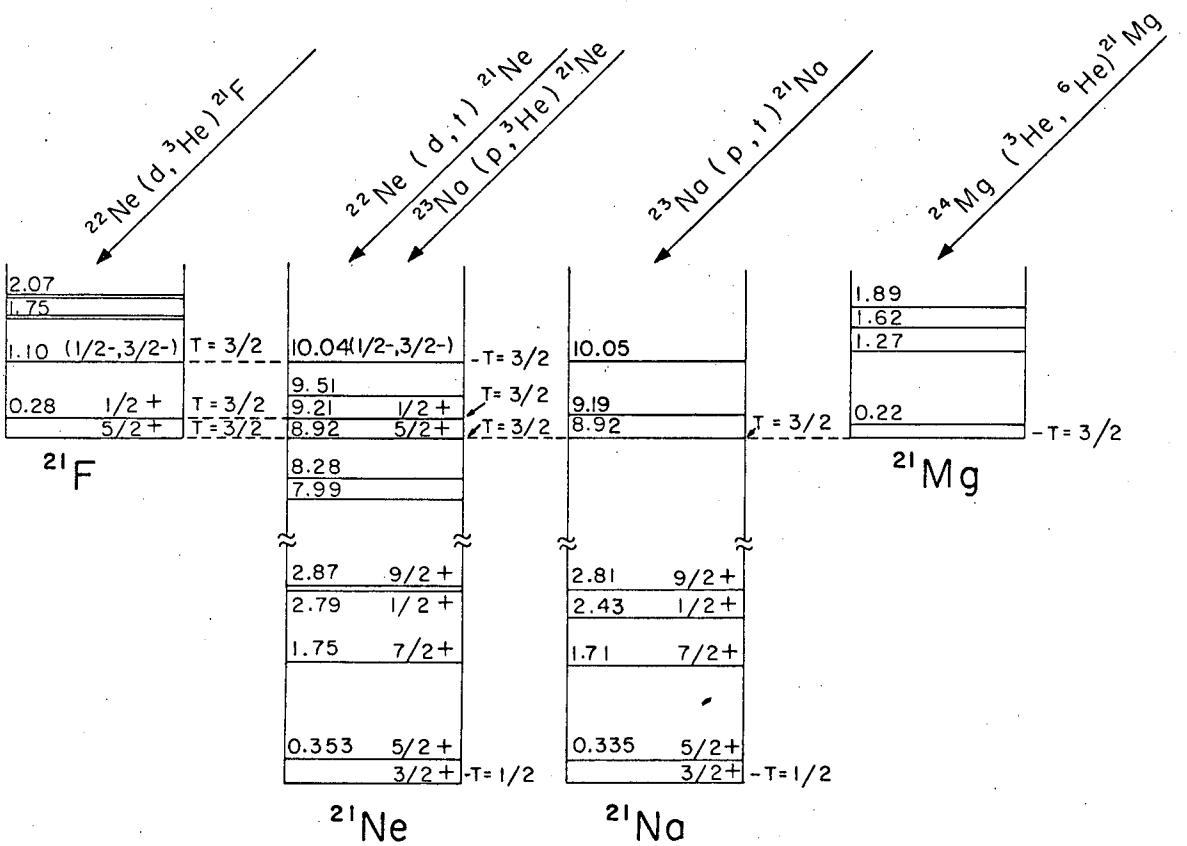
^{22}Ne (d, ^{3}He) ^{21}F
^{22}Ne (d, t) ^{21}Ne
^{23}Na (p, ^{3}He) ^{21}Ne
^{23}Na (p, t) ^{21}Na
^{24}Mg (^{3}He, ^{6}He) ^{21}Mg
2.07
1.75
1.10 (1/2-,3/2-) T = 3/2
0.28 1/2 + T = 3/2
5/2 + T = 3/2
^{21}F
10.04(1/2-,3/2-) -T= 3/2
9.51
9.21 1/2 + T= 3/2
8.92 5/2+ T= 3/2
8.28
7.99
2.87 9/2+
2.79 1/2 +
1.75 7/2+
0.353 5/2 +
3/2 + -T= 1/2
^{21}Ne
10.05
9.19
8.92 T = 3/2
2.81 9/2+
2.43 1/2+
1.71 7/2+
0.335 5/2+
3/2+ -T=1/2
^{21}Na
1.89
1.62
1.27
0.22 -T= 3/2
^{21}Mg
MUB-14100A

Fig. 23.

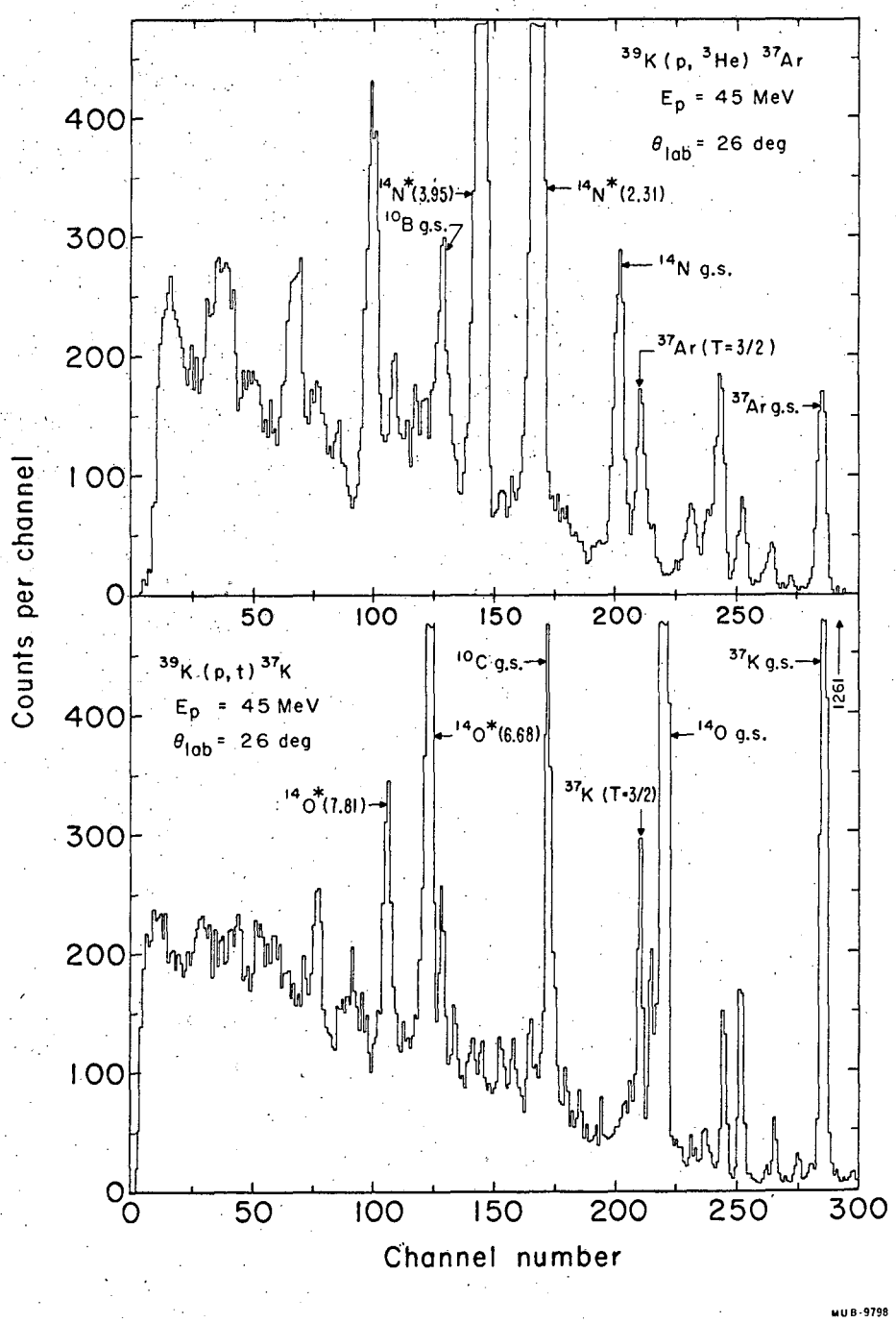
^{39}K (p, ^{3}He) ^{37}Ar
E_p = 45 MeV
θ_{lab} = 26 deg
^{14}N*(3.95)
^{10}B g.s.
^{14}N*(2.31)
^{14}N g.s.
^{37}Ar (T=3/2)
^{37}Ar g.s.
^{39}K (p, t) ^{37}K
E_p = 45 MeV
θ_{lab} = 26 deg
^{10}C g.s.
^{14}O*(6.68)
^{14}O*(7.81)
^{37}K (T=3/2)
^{14}O g.s.
^{37}K g.s.
1261
Counts per channel
Channel number
MUB-9798

Fig. 24.

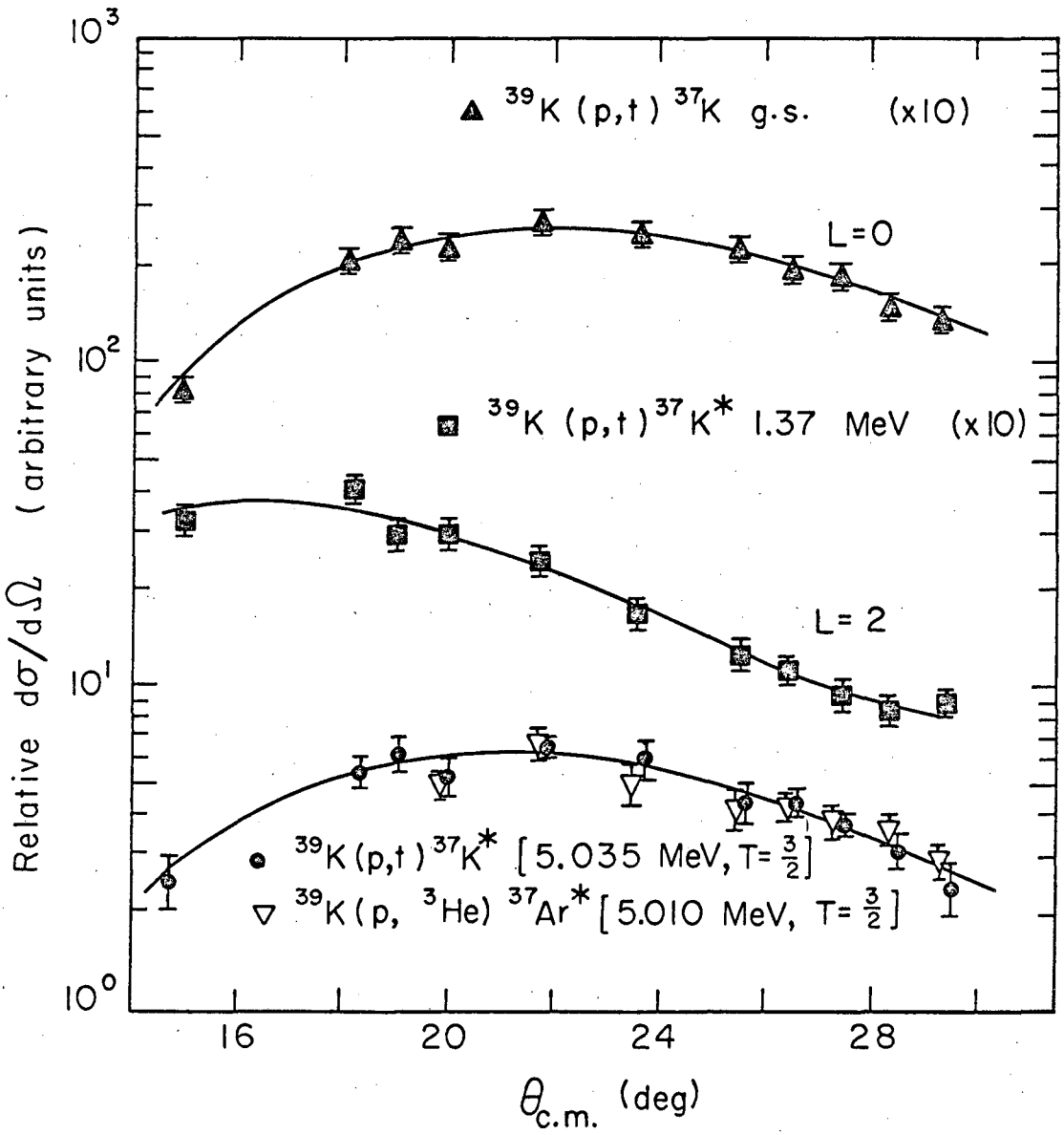

Fig. 25.

XBL675-2990

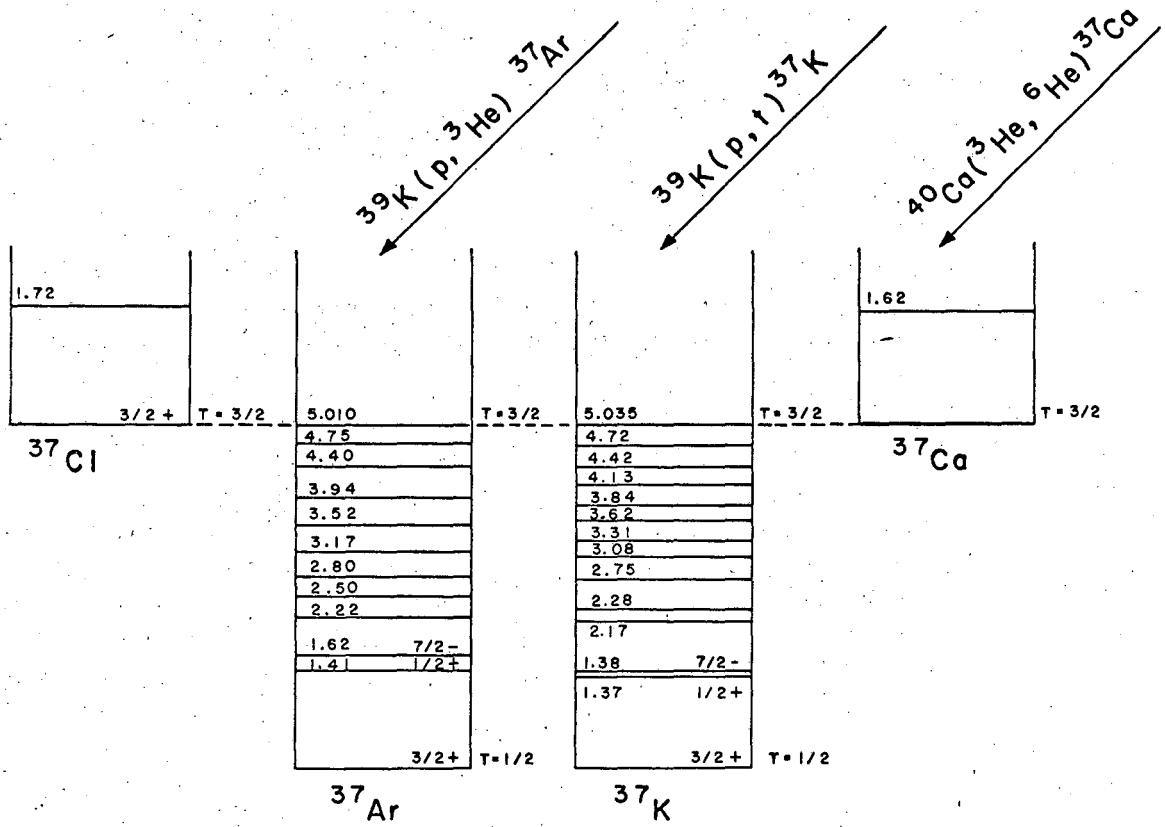
39K(p, 3He) 37Ar
39K(p, t) 37K
40Ca(3He, 6He) 37Ca
1.72
3/2 +
T = 3/2
37Cl
5.010
4.75
4.40
3.94
3.52
3.17
2.80
2.50
2.22
1.62 7/2-
1.41 1/2+
3/2+
T=1/2
37Ar
5.035
4.72
4.42
4.13
3.84
3.62
3.31
3.08
2.75
2.28
2.17
1.38 7/2-
1.37 1/2+
3/2+
T=1/2
37K
1.62
37Ca
XBL675-2993

Fig. 26.